Luiz Guilherme de Souza Schweitzer

LASER CLADDING FOR EPITAXIAL NICKEL BASE SUPERALLOYS TURBINE BLADES

Dissertação submetida ao Programa de Pós-Graduação em Engenharia Mecânica da Universidade Federal de Santa Catarina para a obtenção do Grau de Mestre em Engenharia Mecânica.
Orientador: Prof. Dr.-Ing Walter Lindolfo Weingaertner.

Florianópolis
2014

Ficha de identificação da obra elaborada pelo autor através do Programa de Geração Automática da Biblioteca Universitária da UFSC.

De Souza Schweitzer, Luiz Guilherme
Laser cladding for epitaxial nickel base superalloys turbine blades / Luiz Guilherme De Souza Schweitzer ; orientador, Walter Lindolfo Weingaertner - Florianópolis, SC, 2014. 144 p.

Dissertação (mestrado) - Universidade Federal de Santa Catarina, Centro Tecnológico. Programa de Pós-Graduação em Engenharia Mecânica.

Inclui referências

1. Engenharia Mecânica. 2. Laser cladding. 3. Epitaxial solidification. 4. Turbine blades. I. Weingaertner, Walter Lindolfo. II. Universidade Federal de Santa Catarina. Programa de Pós-Graduação em Engenharia Mecânica. III. Título.

Luiz Guilherme de Souza Schweitzer

LASER CLADDING FOR EPITAXIAL NICKEL BASE SUPERALLOY TURBINE BLADES

Esta dissertação foi julgada adequada para obtenção do Título de Mestre, e aprovada em sua forma final pelo POSMEC

Florianópolis, 23 de Abril de 2014.

_____

Prof. Armando Albertazzi, Dr. Eng
Coordenador do POSMEC

Banca:

_____

Prof. Dr.-Ing Walter Lindolfo Weingaertner
Orientador
Universidade Federal de Santa Catarina

_____

Prof. Rolf Bertrand Schroeter, Dr. Eng.
Universidade Federal de Santa Catarina

_____

Prof. Dr. Rer. Nat. Alexandre Lago
Universidade Federal de Santa Catarina

_____

Prof. Wagner de Rossi, Dr.
Universidade de São Paulo

Dedico este trabalho aos meus pais, pessoas maravilhosas e exemplos de vida.

ACKNOWLEDGMENT

To my family for all the support and incentive they gave me during the last year for the Master Degree in Mechanical Engineering.

To Aline Pires for the love and partnership even separated by nothing less than the Atlantic.

To Prof. Dr-Ing Walter Lindolfo Weingaertner for believing in my capacities, offering me the opportunity in the Laser Zentrum Hannover (LZH) and many years of academic supervision.

To Prof. Rolf Schroeter, Prof. Alexandre Lago and Prof. Wagner de Rossi for the evaluation and correction of this thesis.

To the OFT group from LZH for the support and good laughs in our “Brotzeit”.

To my coworkers and friends from LMP-UFSC.

To the financial support of the Deutsche Forschungsgemeinschaft (German Research Association - DFG) within the Sonderforschungsbereich 871 (Collaborative Research Center) for product regeneration.

To CAPES and POSMEC for the financial support.

For my friends that helped me out when I needed and with whom I could also cheer many good times.

„Ich will die Menschen den Sinn ihres Seins lehren: welcher ist der Übermensch, der Blitz aus der dunklen Wolke Mensch“

(Friedrich Nietzsche, 1896)

RESUMO

A prosperidade e larga utilização da aviação como meio de transporte civil, nacional e internacional, exige seriedade no condicionamento das aeronaves. A manutenção preventiva é um ponto fundamental para que sejam evitados desastres aéreos. A verificação dos motores é indispensável e, devido ao alto valor agregado, corresponde aos custos mais elevados de recondicionamento. As turbinas, por estarem sujeitas a elevada temperatura e pressão, geralmente apresentam o maior número de componentes danificados. Por esta razão há o interesse no desenvolvimento de técnicas para o reparo eficaz de pás de turbina. Erosão e formação de trincas são danos comuns que necessitam de recondicionamento. A recente aplicação de pás monocristalinas (SX), no lugar de policristalinas, apresenta vantagens por suportar melhor as elevadas temperaturas e com isto aumentar a eficiência dos motores [1, 2]. No entanto, não há um método reconhecido para o reparo das pás monocristalinas. A proposta deste trabalho consiste na aplicação de *laser cladding* com injeção de pó, devido a características como o tratamento localizado e controle de material fornecido. Este processo é apropriado devido principalmente à flexibilidade e baixo nível de diluição. Foram desenvolvidos dois métodos para promover o reparo de tais defeitos. Um método consiste na remoção completa de camadas de material onde estão situadas as trincas. O outro prevê a remoção de apenas um pequeno volume da estrutura afetada, através de um entalhe que retira o volume danificado. Com isto, a perda de material, o tempo de trabalho e os custos de manutenção podem ser drasticamente reduzidos. O entalhe tem de ser soldável e também permitir a solidificação de material no mesmo plano orientado como a microestrutura inicial. Para isto, um gradiente de temperatura deve ser introduzido a fim de orientar o crescimento de grão. No entanto, existem desafios para alcançar uma estrutura de cristal único sem rachaduras e poros, devido à distribuição de energia no interior do entalhe. Progressos atingidos e novos desafios são apresentados neste trabalho.

Palavras-chave: *Laser cladding*. Solidificação epitaxial. Pás de turbina.

ABSTRACT

The prosperity and widespread use of aviation as a civil national and international transport requires seriousness in the aircraft conditioning. Preventive maintenance is the key to avoid disasters. For that, is essential the check of engines, which corresponds to the higher reconditioning costs. The turbines, due to elevated temperature and pressure, usually have the highest number of damaged parts. For this reason, there is an interest in developing techniques for the efficient repair of turbine blades. Erosion and crack formation are common damages that require refurbishing. The recent application of single crystal (SX) turbine blades, instead of polycrystalline, present better withstands in high temperatures and thus increases the efficiency of the engines [1, 2]. However, a recognized method for the repair of SX turbine blades has to be developed. The proposal of this work involves the application of laser cladding with powder injection, due to characteristics such as localized treatment and control of the material injected. This process is particularly suitable due to flexibility and low dilution levels. There are two techniques developed to promote the repair of such defects. One way is by the removal of complete layers in which the cracks are located. Another possibility is to remove just a small volume of the affected microstructure. Therewith the loss of material and working time may be drastically reduced as well as the maintenance costs. The notch must be weldable and permit the material solidification in the same oriented plane as the original structure. For that, a temperature gradient has to be introduced in order to guide the grain growth. However, there are challenges to achieve a SX structure without cracks and pores due to energy distribution inside the notch. Current achievements and further challenges are presented in this work.

Keywords: Laser cladding. Epitaxial solidification. Turbine blades.

LIST OF FIGURES

LIST OF TABLES

LIST OF ABBREVIATIONS

BCC	Body Centered Cubic
BR	Beam Radius
CD	Cooling Distance
TE	Temperature
CC	Conventional Cast
DMD	Direct Metal Deposition
DS	Directionally Solidified
EBSD	Electron Backscattered Diffraction
EDX	Energy Dispersive X-Ray
FCC	Face Centered Cubic
HAZ	Heat Affected Zone
LAM	Laser Additive Manufacturing
LI	Laser Beam Intensity
LMD	Laser Metal Deposition
NT	Notch
PD	Powder Quantity
PH	Pre-heating
PUR	Powder Usage Ratio
SA	Sample
SEM	Scanning Electron Microscopy
SLM	Selective Laser Melting
SS	Scanning Speed
SX	Single crystal

LIST OF SYMBOLS

γ	Face-centered cubic phase
γ'	Precipitation phase
M^2	Beam quality factor
θ	Beam divergence
λ	Wavelength
D_0	Beam waist
d_0	Beam spot
d_L	Beam diameter
a	Hatching distance
b	Track width
h	Track height over the surface
h'	Depth of melt pool
I	Beam intensity
P_L	Laser power
A_L	Laser beam profile or area
E_{St}	Energy input per unit length
v	Scanning speed
O_{Sp}	Overlap ratio
m	Powder quantity
θ_x	Stress
h_t	Track height
γ_{LC}	Surface energies of liquid-crystal interface
γ_{LS}	Surface energies of liquid-substrate interface
γ_{CS}	Surface energies of crystal-substrate interface
ΔG	Nucleation activation energy
T_m	Equilibrium melting temperature
ΔH_m	Latent heat of melting
ΔT	Undercooling below T_m
θ_S	Contact angle
B_s	Magnetic field intensity
U_{is}	Solenoid voltage
f_s	Solenoid frequency
N_s	Number of solenoids
r_s	Distance from solenoids to the induction coil
$\sigma_{\gamma-\gamma'}$	Interface energy between phases
ΔG_V	Volume free energy difference
ΔG_ε	Strain free energy difference
ΔG_M	Magnetic free energy difference

SUMMARY

1 INTRODUCTION

The preventive maintenance is essential to proportionate the required security patterns for airplanes. It is crucial to have the engines regularly checked in order to repair damaged components. The engine mostly used in civil airplanes is the turbofan, which can be divided into six main parts, shown in Figure 1.1. Through the fan occurs the air admission for cooling (70%) and combustion (30%). The air for combustion is submitted to two compression stages before entering the combustion chamber. After the combustion, the high-pressure air collides against the turbine blades in the high-pressure turbine and then in the low-pressure turbine. As a result of extreme temperature and pressure, the turbine blades are the components usually replaced during the maintenance [3].

Figure 1.1 – Turbofan engine with six stages for civil airplanes.

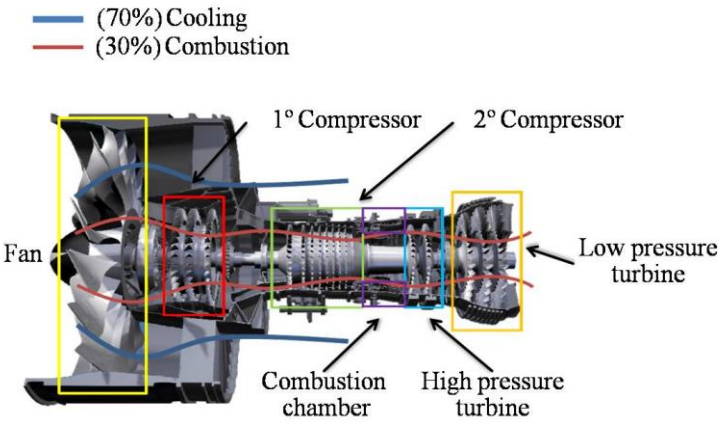

SOURCE: Bräuling [3].

Recently, single crystal (SX) superalloy nickel base turbine blades started to be used in the high-pressure turbine due to better withstands working in such conditions. Nickel base superalloys are a class of especial metallic materials that can combine high temperature strength, toughness and resistance to degradation in corrosive or oxidizing environments. Due to these characteristics, such materials are mostly used in aircraft and power generation turbines. The intensive research and process development have resulted in alloys that tolerate

average temperatures of 1050°C and peaks of 1200°C (local hot spots), which corresponds to 85 % of the material melting point [1].

It is most extensively applied in the combustor and turbine sections with elevated temperatures, which typically constitutes from 40 % to 50 % of the total weight of an aircraft engine. Concerning the microstructure, these components may contain equiaxed grains or be cast as single crystal (SX). The advantage of SX microstructure is the elimination of high-angle grain boundaries, which are sites for damage at high temperatures. The manufacturing of SX turbine blades is typically performed by complex casting procedures that counts on cooling schemes to control the grain growth. Superalloys consist of a Ni-base austenitic phase (γ), which usually contains a high percentage of solid solution elements and a large volume fraction of coherent Ni_3Al and Ni_3Ti intermetallic precipitates (γ'). This contributes largely to the alloy strengthening [2, 3].

The negative point of this technology is the high manufacturing costs of SX components. The frequent need to replace the blades due to limited lifetime increases the operation costs of engines. Typical turbine blades maintenance reasons are thermomechanical cracks and tip erosion, which leads to the loss of engine efficiency [5]. Due to the extreme operating conditions and safety-related regulations, the regeneration of defective turbine blades for flight operations requires special treatments. However, a large number of defective parts are no longer suitable to this regeneration process because the defects exceed the manufacture's authorization. The restriction is based on, among other reasons, the fact that there is currently no adequate method to restore the original material properties.

The manufacture of the original SX parts in the industry is mostly made through the Bridgman-method. It corresponds to a vacuum investment casting process in which the component is cooled uniformly in a furnace to induce the solidification according to a directional heat flow [6]. There is a great interest on the development of repair techniques to extend the life of SX components and the challenge is to generate a method that achieves the solidification with a structure similar to the original part. For that, it is necessary to build up an environment with similar conditions to achieve the required microstructure. The introduction of a cooling and heating unit is a way to reach a temperature gradient in a defined direction. Regarding the process itself, the laser cladding with powder injection is suitable because of key advantages such as operation of complex geometries, low dilution levels and high process flexibility. Laser cladding

corresponds to a Laser Additive Manufacturing (LAM) process that uses the electromagnetic radiation of a laser beam to form a melt pool through the deposition of a thin layer of material, called “clad”, on a substrate [7].

The project is funded by the *Deutsche Forschungs-gemeinschaft* (German Research Association - DFG) within the *Sonderforschungsbereich* (SFB) 871 (Collaborative Research Center) for product regeneration. This work comprehends one part of the SFB 871, which corresponds to a study to investigate the influence of various cladding parameters on the microstructure formation in order to achieve the SX cladding from the nickel base superalloy CMSX-4. The main goal is the development of a method to repair the tip of damaged SX turbine blades and to reduce the maintenance costs.

This master thesis is a result of cooperation between the *Laboratório de Mecânica de Precisão (LMP) – Universidade Federal de Santa Catarina (UFSC)* and the *Laser Zentrum Hannover (LZH) – Leibniz Universität Hannover*. The credits for the master degree were obtained according to the POSMEC (*Programa de Pós-Graduação em Engenharia Mecânica*) at UFSC, Florianópolis/Brazil, and the experiments were performed under the supervision of Boris Rottwinkel in Hannover/Germany.

2 STATE OF THE ART

2.1 LASER TECHNOLOGY

Laser corresponds to an acronym that stands for “Light Amplification Stimulated Emission of Radiation”. There are some particularities of the laser light that differentiates it from all other lights and proportionate a wide range of applications. These characteristics are a narrow laser beam, a defined color and aligned waves. A laser system usually works with energy in the form of electricity as input, which stimulates a medium and generates light. Generally, the energetic efficiency is low; however, the narrow beam produced compensates it [8].

The beam quality of a laser is usually measured with the M^2 factor, also called beam quality factor or beam propagation factor. M^2 is a value that indicates how close a laser is to be a single mode TEM_{00} beam, which in turn determines how small a beam waist can be focused.

Figure 2.1 – Beam characteristics.

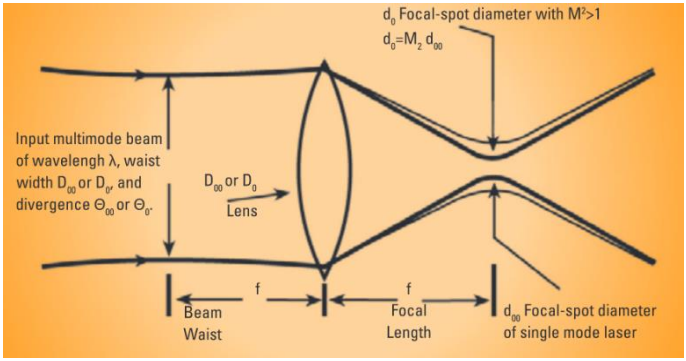

SOURCE: Ophir[9].

The ISO/DIS 11146 [10] requires that M^2 has to be calculated from a series of measurements on real beams by focusing with a fixed position lens of known focal length, and then measuring the characteristics of the artificially created beam waist and divergence. For the perfect Gaussian TEM_{00} condition, M^2 is equal to 1. For laser beam propagation through space, the equation for the divergence, θ, of an unfocused beam is given by:

$$\theta = \frac{M^2 \cdot 4 \cdot \lambda}{\pi \cdot D_0} \quad (1)$$

Where,

θ - Beam divergence
M^2 - Beam quality factor
λ - Wavelength
D_0 - Beam Waist

SOURCE: Hitz [8].

In the case of a pure Gaussian TEM_{00} beam, M^2 equals to 1, and thus the minimal beam spot is:

$$d_0 = \frac{4 \cdot \lambda}{\pi \cdot \theta} \quad (2)$$

Where,

d_0 - Minimal beam spot
λ - Wavelength
θ - Beam divergence

SOURCE: Hitz [8].

For real beams, M^2 will be larger than 1, and thus the minimum beam waist will be larger by the M^2 factor.

There are several sources and each has a different working method. In Table 2.1 is shown four sources:

Table 2.1 – Laser types.

Source	**λ [nm]**	**Max. Power [kW]**	**Efficiency [%]**	**Power density [MW/cm^2]**
CO_2	10600	20	<10 %	64
Fibre	1000 - 1100	50	<30 %	995
Nd:YAG	1064	10	<12 %	32
Diode	800 - 1030	10	<40 %	1,3

SOURCE: Kaierle [11].

CO_2 laser

A carbon dioxide laser is based on a gas mixture as gain medium. It contains carbon dioxide (CO_2), helium (He), nitrogen (N_2), possibly hydrogen (H_2), and water vapor and/or xenon (Xe). The system is pumped via gas discharge. The nitrogen molecules are excited by the discharge into a metastable vibrational level and by collision, this energy is transferred to the CO_2 molecules. Helium is basically used for cooling the other elements, such as hydrogen. It also reoxidize the carbon monoxide (formed in the discharge) to carbon dioxide [12]. A particularity of CO_2 lasers it that the beam guidance has to be performed with mirror optics.

Fiber laser

Fiber lasers uses an optical fiber doped with rare earth ions as gain media, such as erbium (Er^{3+}), neodymium (Nd^{3+}), ytterbium (Yb^{3+}), thulium (Tm^{3+}), or praseodymium (Pr^{3+}). The stimulation is made by fiber-coupled laser diodes. In Figure 2.2 is presented the setup of a simple fiber laser. Pump light is introduced from the laser diode on the left side through a dichroic mirror into the core of the doped fiber. The laser light is generated and is extracted on the right side.

Figure 2.2 – Setup of a fiber laser.

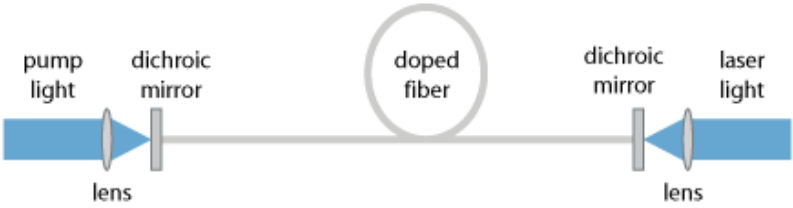

SOURCE: Tünnermann *et al.* [13].

Nd:YAG

YAG laser is usually used for solid-state lasers based on neodymium-doped YAG (Nd:YAG, more precisely Nd^{3+}:YAG), although there are other rare-earth-doped YAG crystals, such as ytterbium, erbium, thulium or holmium. YAG is the acronym for yttrium aluminum garnet ($Y_3Al_5O_{12}$), a synthetic crystal material that became popular in the form of laser crystals in the 1960s. The Nd:YAG lasers are optically pumped using a flash tube or laser diodes.

Figure 2.3 – Nd:YAG laser rod.

SOURCE: Chaoyang *et al.* [14].

Diode laser

The diode lasers are the most common type of laser produced. It has a very wide range of use, like for example fiber optic communications, barcode readers, laser pointers, CD/DVD/Blue-ray reading and recording devices, printing, scanning, etc. Those applications come from the flexibility of laser diodes, which are much lighter, smaller, and more rugged than other laser systems [8].

A laser diode is formed by the junction of two dissimilar types of semiconductors (n-doped and p-doped). In an n-doped semiconductor, there are extra electrons that are the charge carriers. In a p-doped semiconductor, there are extra holes that are the charge carriers. In a diode laser, the light emission occurs at the junction of an n-doped and a p-doped material. When both materials are in contact, some of the n-doped material electrons move across the junction and combine with some of the p-doped material's holes, and vice-versa (Figure 2.4 – left). The hole is a place where there is supposed to be an electron, for that reason an electron and a hole combine. In this combination, the electron loses energy, which is liberated as heat and photon. At the beginning, a number of charge carriers move across the junction to combine with the opposite charges. However, it reaches a point of an excess of positive charge on the n-doped material, and an excess of negative charge on the p-doped. By this time, there are no more carriers moving across the junction (Figure 2.4 – right) [8].

Figure 2.4 – Junction of p-doped and n-doped semiconductor material.

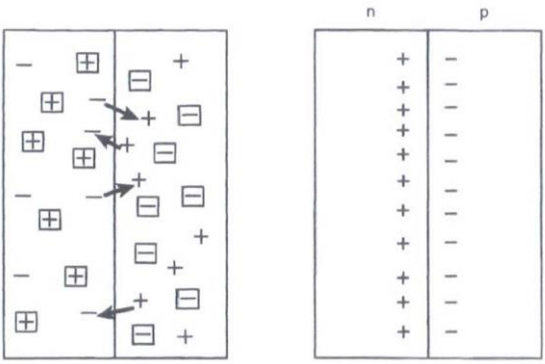

SOURCE: Hitz *et al.* [8].

To prolong the cross of carriers, mobile charges are injected, as shown in Figure 2.5. This creates a steady-state condition in which photons are continuously being emitted from the junction. In order to enhance the power produced by diode laser systems, diode bars are used in high-power diode laser, which contains an array of broad-area emitters. Broad area laser diodes are edge-emitting with a shape of a broad stripe [15].

Figure 2.5 – Movement of electrons and holes through the junction of a semiconductor.

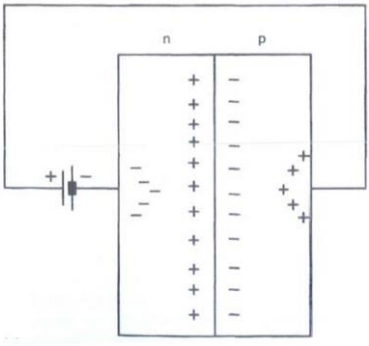

SOURCE: Hitz *et al.* [8].

The reason for the use of diode arrays instead of single emitters is that those arrays can be operated with a more stable mode profile, consisting of one so-called beam let from each emitter. There are several techniques that exploit some degree of coherent coupling of neighbored emitters, leading to better beam quality. Such techniques include those directly applied in the fabrication of the diode bars and others involving external cavities [16].

Figure 2.6 – Diode laser array.

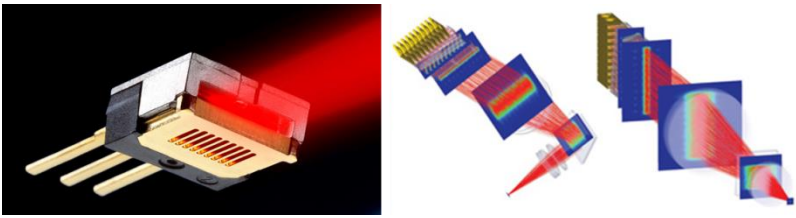

SOURCE: Kaierle [11].

The relevant design parameters of diode bars are the number of emitters, their width and spacing. Concerning the beam quality and brightness, it is ideal to get the output power from a small number of closely spaced emitters. In addition, closely spaced emitters are more difficult to be cooled, at least in continuous wave operation. The array geometry makes diode bars very suitable for methods of coherent or spectral beam combining, which allows a higher beam quality [17].

2.2 LASER CLADDING

Laser cladding and Selective Laser Melting (SLM) are Laser Additive Manufacturing (LAM) processes with powder (or wire) materials. The electromagnetic radiation of a laser beam is absorbed by the surface, creating a melt pool in which the laser is used as heat source to deposit a thin layer of material, called “clad”, on a substrate [7]. Some characteristics of LAM processes are:

- Low dilution
- Minimal distortion
- Small heat affected zone (HAZ)

- High heating and cooling rates
- Uniformity of layers
- Good fusion bond
- Adaptable to automated processes

LAM techniques may be classified according to the method used for material supply into the working surface: two stages (SLM with preplaced powder) and one stage (Laser cladding with delivered powder or wire feeding) [7].

Two-stage process

The process is divided into two stages; the first consists on powder placement over the surface and in the second this powder is melt by laser irradiation. This process corresponds to the selective laser melting, in which a "powder bed" is formed on the substrate surface, as Figure 2.7 shows.

Figure 2.7 – Two-stage process.

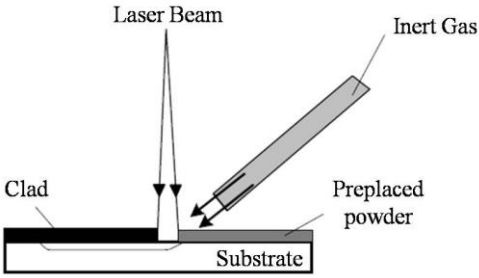

SOURCE: Toyserkani *et al.* [7].

The pre-placed powder cladding can be used as a method for coating and prototyping. There are some particularities about its usage, such as the homogeneous dispersion of powder over the surface in order to have an equal adhesion and not introduce stresses into the new structure. The powder should also remain in the same position during the process, even with the action of shielding gas. For that, chemical binders may be mixed with the powder to ensure the cohesion of the grain powder to the substrate. The side effect is the possible formation

of porosity due to evaporation of those chemicals during the process [18].

The process schema of a SLM process made from a CAD model is shown in Figure 2.8. The model is sliced into a defined number of layers and the laser beam melts each layer of deposited powder material. After cooling down and solidifying, the "bed" is lowered to enable addition of material for the next layer, which is again melted by the laser beam. This procedure is repeated until the part is finished [19].

Figure 2.8 – Selective Laser Melting.

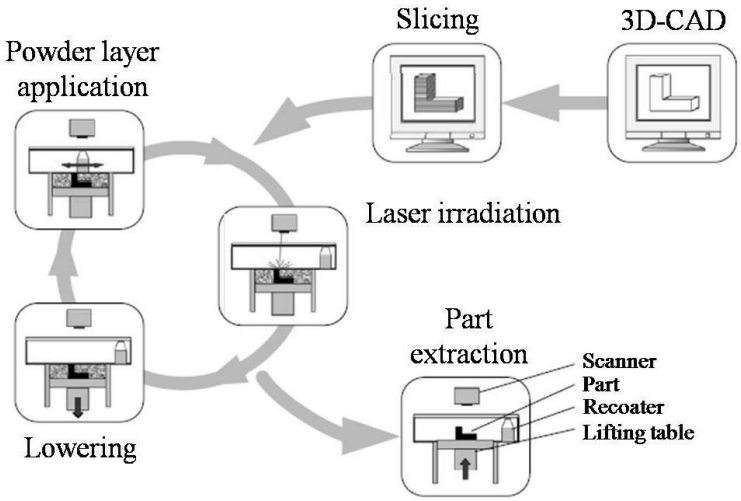

SOURCE: Meiners [19].

One-stage process

The basic difference in the one-stage process is that the additive material is fed into the substrate and simultaneously melted by the laser beam. Laser cladding is used as term for this process, but in the literature it may also be called Laser Metal Deposition (LMD) or Direct Metal Deposition (DMD). The laser cladding provides several advantages over the two-stage process, such as:

- Operation of complex geometries due to the capability of material supply into the melt zone

- ❖ Efficiency for large areas due to the application of several adjacent tracks
- ❖ Require no tooling or molds
- ❖ Construction and repair of high-valued parts in a cost-effective manner
- ❖ Contraction of clad layers by cooling can be corrected through material feeding in the overlap of the next track
- ❖ Coating thickness may be changed during the process through the scanning speed (just for powder injection)

The addition of material may be realized by wire feeding or powder injection as shown in Figure 2.9.

Figure 2.9 – Laser cladding with wire (left) and powder (right).

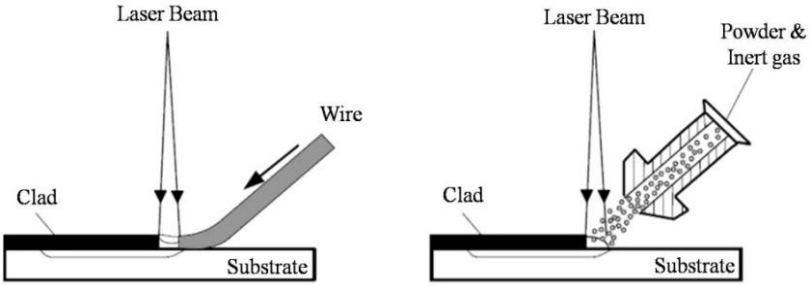

SOURCE: Toyserkani *et al.* [7].

The wire feeding is mostly applied in situations where the geometry favors one single clad, such as rotationally symmetric components. The nozzle must be close to the working area to permit an exact wire supply into the laser spot. There is also possible to apply preheating into the wire to enhance the process efficiency [20, 21].

Despite the functionality of wire feeding, the powder technique is a much more common method, mostly because of the flexibility due to the following reasons [22, 23]:

- ❖ Permits to vary the material quantity and composition during the process
- ❖ Availability of more alloys as powder then as wire

- ❖ The laser beam is not obstructed by the powder flow as it can be by the wire

The powder is stored free off atmospheric influence in a feeder, which delivers it through flexible tubes. Those forward the powder until the nozzle, where it is directed to the working area.

2.2.1 POWDER FEEDER

The powder feeder is responsible for delivering the desired amount of material to the working area. There are different strategies for it, depending on the material characteristics, for instance, mesh size, required feed rate and the interaction between the grains to each other. Different types of powder feeders can be used in the laser cladding process. Several designs have been developed to provide the smooth and steady flow in the required flow rates, according to the powder used. They may be classified according to the operation principle as Table 2.2 and Figure 2.10 shows:

Table 2.2 – Powder feeder.

	Operation principle	Powder flows through […]	Control
A	Gravity	[…] an orifice under the hopper	Dimension of the hole
B	Gravity	[…] the hole into the rotating disk, turn for 180 degrees and leave by the other hole	Dimension of the hole and disk speed
C	Gravity	[…] the holes of a metering wheel	Dimension of the holes and angular speed
D	Gravity	[…] a lobe gear	Gear rotation

E	Mechanical	[…] the screw	Screw size and rotation
F	Fluidized bed	[…] the gas	Apertures to let the particles leave the chamber

SOURCE: Carvalho *et al.* [24], Weck *et al.* [25].

It is also possible to combine the methods above mentioned in order to achieve more stability in the powder stream. Despite the working principle, every feeder needs a carrier gas (argon, helium, nitrogen) to transport the powder from the storage to the desired location.

Figure 2.10 – Powder feeder.

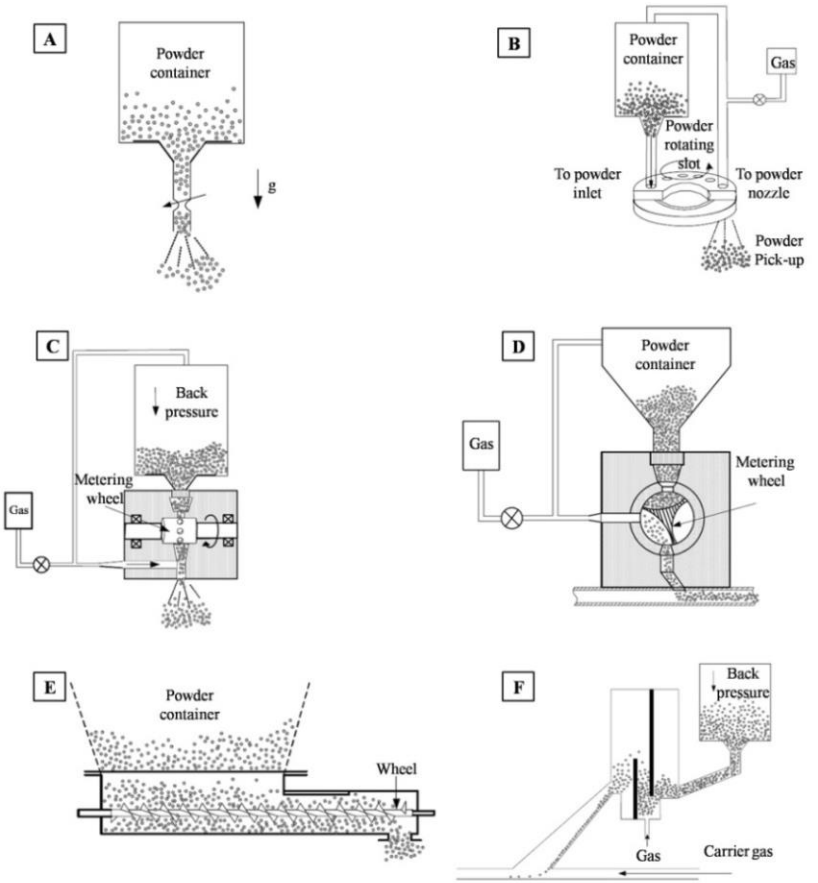

SOURCE: Huron [26].

2.2.2 NOZZLE

In laser cladding, the powder injection may be conducted by two nozzle configurations: coaxial and lateral. The basic layout of these two designs is shown in Figure 2.11, from which derived several invented types of nozzles. For instance, Islam *et al.* [27] invented a multiple nozzle processing head for manufacturing and repairing of turbine

blades and compressor components. Jeantette *et al.* [28] developed a coaxial nozzle to be applied into the production of complex shapes.

In both types, coaxial and lateral, the powder may be preheated in order to increase its efficiency. An advantage of the coaxial over the lateral nozzle is the freedom for motion, since it may be coupled with the optical system. It also achieves better powder efficiency. The powder stream is formed by a combination of the shield and shaping gas in order to achieve a homogeneous distribution. The nozzle tip also plays an important role by the formation of different powder stream profiles and powder focus points [29].

Figure 2.11 – Coaxial nozzle setup.

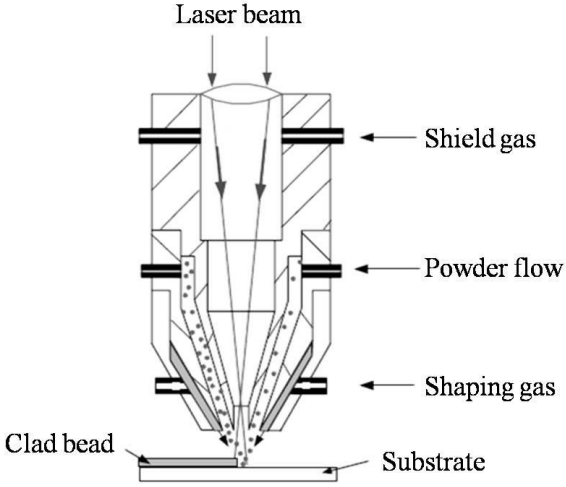

SOURCE: Toyserkani *et al.* [7].

In order to achieve good powder efficiency, the powder stream's focus point must be at the level of the melt pool. The interaction of powder particles with the laser beam and the inert gas in the melt pool are important aspects to achieve a quality clad. The powder interaction with the surface may produce different phenomena as [30]:

- Solid particles may ricochet into solid surfaces
- Solid or liquid particles cause catchment with a liquid surface

- ❖ Liquid particles cause catchment with a solid surface

The nozzle type, powder stream, powder profile in the process zone, and powder stream diameter in the melt pool affect the interaction of particles on the working surface. An efficient nozzle reduces the impact of solid particles against a solid surface in order to increase the powder catchment efficiency.

2.2.3 CLAD FORMATION

In Figure 2.12 is shown the simplification of the laser cladding process and some general characteristics. The clad geometry is a result of the parameters used such as laser power, scanning speed, etc. Several authors have studied the laser cladding process by means of a simple parameter variation for a fixed material combination [31, 32]. In that way is possible to define the correlation between the most influential variables, which are at disposal in Figure 2.13.

Figure 2.12 – Clad formation by lateral overlapping.

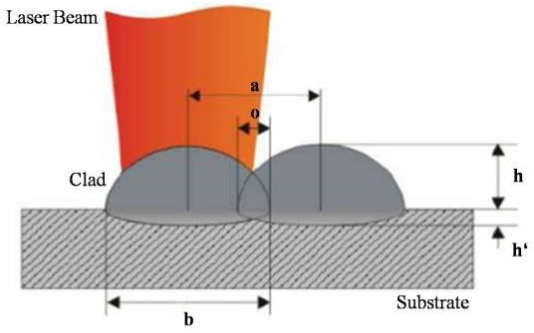

a	hatching distance
b	track width
h	track height
h‘	depth of melting pool
o	overlap

SOURCE: Kaierle *et al.* [33].

From the parameters above mentioned and equations 3 to 5, some characteristics may be defined. The laser beam intensity (Eq.3), where P_L is the laser power and A_L the laser beam profile (area). The energy input per unit length (Eq.4), where *v* is the scanning speed. In addition, the overlap ratio (Eq.5), where *a* is the hatching distance and *b* represents the track width (Figure 2.12).

$$I = \frac{P_L}{A_L} \tag{3}$$

Where,

I - Laser beam intensity
P_L - Laser power
A_L - Laser beam profile

SOURCE: Kaierle *et al.* [33].

$$E_{Sl} = \frac{P_L}{v} \tag{4}$$

Where,

E_{Sl} - Energy input per unit length
P_L - Laser power
v - Scanning speed

SOURCE: Kaierle *et al.* [33].

$$O_{Sp} = \frac{b - a}{b} \tag{5}$$

Where,

O_{Sp} - Overlap radio
b - track width
a - hatching distance

SOURCE: Kaierle *et al.* [33].

Figure 2.13 – Process parameters in laser cladding.

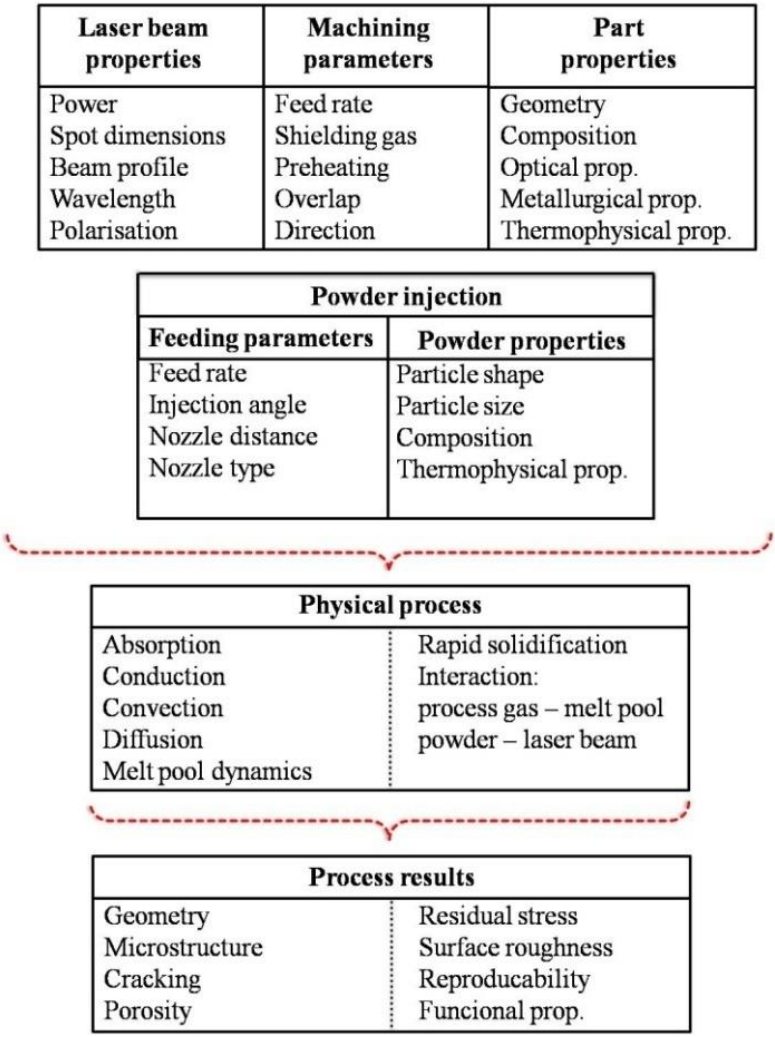

SOURCE: Kaierle *et al.* [33].

Scanning speed (v) and the powder quantity (m) influence the geometry of the clad layer. Cladding thickness depends on the amount of material given to the melt pool during the process. It is usual to combine both parameters to define the powder feed rate as m/v [g/min],

to calculate the amount of powder added to the process per unit time [34, 35]. A linear relation exists between the powder feed rate and the energy required, if sufficient energy is available to melt all arriving powder. Excessively high laser energy input leads to high dilution and undesirable mechanical properties in the material, for example the decrease of wear resistance. Just a small layer of substrate should be melted, which is bonded with the clad material [36].

Lugscheider *et al.* [34] assert that when cladding larger areas by laying single tracks next to each other, the overlap of tracks is considered another process parameter. Too small tracks results on a poor clad formation. The increase of overlap the surface becomes smoother, but every track produces a heat treatment in the preceding track and a heat-affected zone (HAZ) is developed in the clad layer [36].

The cladding microstructure is partly influenced by the structure and size of the powder particle, but mainly affected by the solidification, which depends on process parameters such as power density, absorption of energy and scanning speed [35]. The absorption coefficient is much higher for liquids than for solids. The absorptivity rises significantly when the melting occurs. It is also influenced by the angle of incidence from the beam with respect to the material surface [37].

The laser beam produces a melt pool on the moving substrate and at the same time, the carrier gas introduces the powder for mixing and melting in the liquid. A signal of a good cladding is a small layer of remelted material in the substrate. When the substrate mixes with the cladding material, the clad composition is diluted with certain degradation of the substrate surface properties [36].

The properties of the clad layer itself may be divided into four main groups as shown in Table 2.3. Several from these properties are inter-related, like for example the porosity that is affected by the material homogeneity, dilution and microstructure [39, 40].

Table 2.3 – Clad properties.

Geometrical	**Mechanical**	**Metallurgical**	**Qualitative**
Clad dimension	Hardness	Microstructure	Porosity
Dilution	Residual stress	Dilution	Cracking
Roughness	Wear resistance	Grain size	
	Tensile strength	Homogeneity	
		Corrosion resistance	

SOURCE: Schneider [38].

Residual stress

When a heat source passes a line along a substrate in welding or laser processing, the material will undergo thermal and strain. A butt weld is a way to understand what happens to the material, as shown in Figure 2.14. A section of the material in the weld area experiences different rates of expansion and contraction compared with surrounded area sections. The behavior of this section during a weld thermal cycle, changes in the sections mechanical properties as a function of temperature, for example elastic modulus, Poisson's ratio, etc. The hatched area M-M' is the region where plastic deformation occurs. Section A-A is ahead of the heat source, which is not yet significantly affected by the heat input. The temperature change may be considered zero. Along section B-B, which crosses the heat source, the temperature distribution is very steep and becomes less steep according to the detachment from the heat source in the section C-C. This distribution eventually becomes uniform far from the heat source, along section D-D.

The thermal induced stress σ_x in section A-A may be considered equals to zero due to the inactivity of the heat source in this area. In the section B-B, σ_x is close to zero because of the melt pool, which does not support loads. A compressive σ_x is generated at lower temperatures in the lateral regions from the heat source due to expansion of the heated area [41]. Along section C-C, the weld metal and the adjacent base metal have cooled and hence have a tendency to shrink and produce tensile stress (positive σ_x). Since the distance from the weld increases, the stress first changes to compressive and then becomes tensile. Finally along D-D high tensile stresses are produced in areas near the weld. Since this section is far from the heat source, this stress corresponds to the residual stress distribution [41]. Xiangling *et al.* [42] found that the coating material is exposed to compressive stress and that in HAZ is under tensile stress. Compressive stress at the surface is favorable, but tensile stresses result in premature failure. Those stresses can be adjusted by controlling the power input and the scanning speed of the laser beam over the substrate.

Figure 2.14 – Schematic illustration of changes in temperature and stresses during welding according to different weld sections.

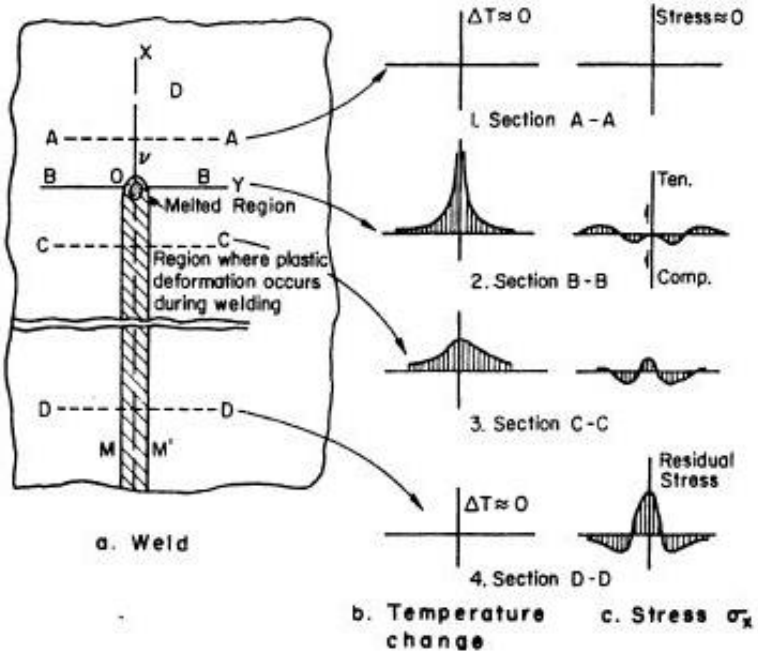

SOURCE: Brenner *et al.* [39].

Dilution

The clad requires a strong fusion between the added material and the substrate, which is achieved through a melt pool formed in the substrate. However, this pool must have the smallest depth possible in order to obtain a layer of the pure, undiluted material.

The dilution of the substrate elements into the layer is an indicator of the clad quality, which can be measured in two ways [43]. One method is based on the geometry of the clad layer as shown in Figure 2.15. The dilution is defined as the ratio of the clad depth (h') in the substrate over the total clad height (h_t). This geometric approach assumes a homogeneous distribution of elements in the clad cross-section.

Figure 2.15 – Single clad layer cross-section with definition of the clad geometry: clad height (h), clad depth (h'), total clad height (ht) and clad width (b).

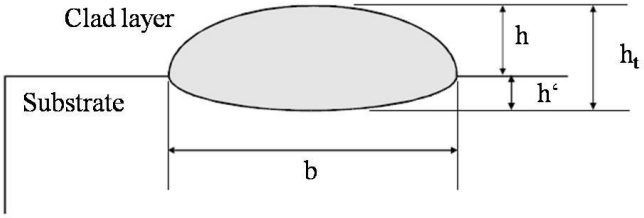

SOURCE: Bruck [43].

The second method consists on analyzing the material composition in the coating layer (chemical or volumetric dilution). A comparison between the clad layer and the substrate defines the general dilution.

Porosity

Porosity is a problem that usually appears in additive manufacturing processes. It may be defined as the presence of gaps into the clad layer, which can be formed in the clad or between adjacent tracks:

- The shielding gas or even chemical reactions during the process may form bubbles that are trapped in the solidifying melt pool
- The contraction resulted from the cooling may introduce tensile stress that form holes in the structure
- The presence of small flaws, such as grease or even chip of previous machining, influences the surface tension and the bonding of coating material to substrate
- Between the overlap of tracks may occur the so-called "inter-run porosity" as shown in Figure 2.16. Some particles do not receive sufficient energy to melt and are deposited in the surrounding of the melt pool [47]

Figure 2.16 – Inter-run porosity.

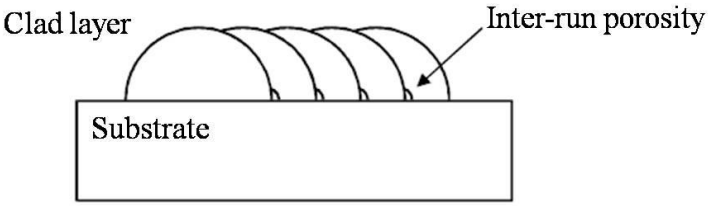

SOURCE: Steen [44].

2.2.4 APPLICATIONS

The repair and refurbishment of high-value parts such as tools, turbine blades and military equipment are important applications of laser cladding. There are conventional methods to restore these damaged components, such as welding. However, the thermal harm potentially results on a component with low mechanical quality, crack and porosity, which leads to a short life. With laser cladding, a permanent structural repair of several alloys is achievable, even of aluminum, which is frequently considered non weldable. The success of laser cladding lies on some characteristics, such as small heat zone, rapid solidification, low dilution and controllability over the depth of the heat-affected zone.

An important application is the recovery of turbine blades, which corresponds to a very promising field to the application of laser cladding. Turbine blades are exposed to high thermal and mechanical stresses in the aggressive operational environment. The appearance of creep, life cycle fatigue, hot corrosion and impact of external on the surface are usually noticed (Figure 2.17). During the maintenance of turbines, the damaged blades have to be substituted in order to guarantee the integrity of the entire equipment. Those parts are the most critical in terms of manufacturing difficulties and costs, which increases the demand for further technology research in this area. The repaired parts have to maintain the mechanical and metallurgical properties of the original ones [45].

Figure 2.17 – Damaged turbine blade.

SOURCE: Pollock *et al.* [45].

Turbine blades are usually made of superalloys, which are highly susceptible to strength loss and physical distortion when exposed to excessive temperature variations. That characteristic restricts the use of conventional methods, such as tungsten inert gas, metal inert gas, plasma and electron beam welding. The temperature increases above certain limits weaken the alloy, causing irreversible damage. In comparison with traditional welding techniques, laser cladding transfers heat in a small and localized area. The reduction of heat input into the component can reach until one order of magnitude lower than the conventional welding, which collaborate to a reduced residual stress and substantially smaller heat affected zone [45].

An even greater market potential exists for the application of laser cladding into repair of gas turbines built with SX components in order to improve the efficiency during the operation at higher turbine inlet temperatures. Not only in the construction, but also in the repair of such components, laser cladding is quoted as the most suitable technology [46, 47].

The market for repair and refurbishment is vast and promising, taking the maintenance of aircraft engine components as an example, in which it corresponds up to 30 percent of the total aircraft maintenance. The global market for repair of aircraft engine turbines and blades, used in civil and military applications, has been estimated to be about 1.2 billion dollars per year [48].

2.3 WELD SOLIDIFICATION

Solidification in welding is directly correlated to the development of the grain structure in the fusion zone and the effect of welding parameters on the grain structure. The grain structure of the fusion zone can significantly affect its susceptibility to solidification cracking during welding and its mechanical properties after welding.

2.3.1 EPITAXIAL GROWTH AT FUSION BOUNDARY

In Figure 2.18 is represented the nucleation of a crystal over a flat substrate. The parameters γ_{LC}, γ_{LS} and γ_{CS} are the surface energy of a liquid-crystal interface, liquid-substrate interface, and crystal-substrate interface, respectively. According to Turnbull [49], the energy barrier ΔG for the crystal to nucleate on the substrate is:

$$\Delta G = \frac{4\pi\gamma_{LC}^3 T_m^2}{3(\Delta H_m \Delta T)^2}(2 - 3cos\theta_s + 3cos^3\theta_s) \quad (6)$$

Where,

ΔG - Nucleation activation energy
γ_{LC} - Surface energy liquid-crystal
T_m - Equilibrium melting temp.
ΔH_m - Latent heat of melting
ΔT - Undercooling below T_m
θ_S - Contact angle

SOURCE: Turnbull [49].

If the liquid wets the substrate completely, θ is zero and so is ΔG, which turns possible to the crystal to nucleate without having to overcome any energy barrier necessary for nucleation.

For fusion welding, the nucleation occurs in the substrate grains at the fusion line. Since the liquid metal of the weld pool is in contact with these grains and wet them completely, there are no difficulties for the nucleation from the liquid metal upon the substrate grains. In Figure 2.19 is shown schematically the epitaxial growth or epitaxial nucleation. The arrow in each grain indicates its <100> direction. For materials with

a face-centered-cubic (FCC) or body-centered-cubic (BCC) crystal structure, the columnar dendrites grow in the <100> direction.

The epitaxial growth in fusion welding was first discovered by Savage *et al*. [50]. With x-ray back-reflection technique, the continuity of crystallographic orientation across the fusion boundary is confirmed. Epitaxial growth can also occur when the workpiece is a material of more than one phase. Elmer *et al*. [51] observed epitaxial growth in electron beam welding of an austenitic stainless steel consisting of both austenite and ferrite. In Figure 2.20, it is shown that both austenite (A) and ferrite (F) grow epitaxially at the fusion line, from the base metal to the weld metal.

Figure 2.18 – Crystal nucleated on a planar substrate from a liquid.

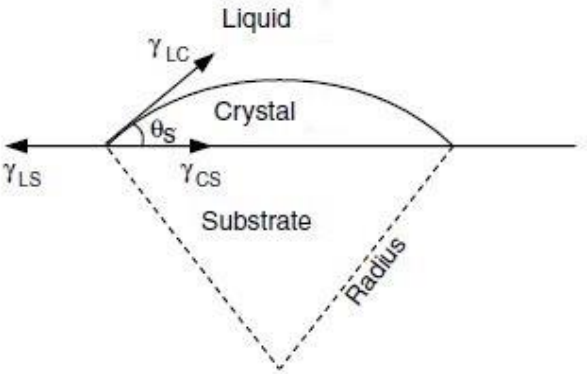

SOURCE: Kou [52].

Figure 2.19 – Epitaxial growth of weld metal near the fusion line.

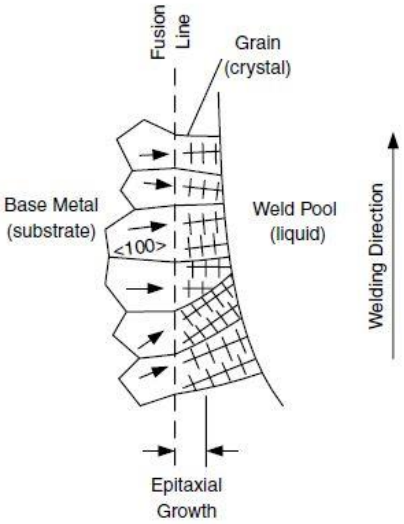

SOURCE: Kou [52].

Figure 2.20 – Epitaxial growth of austenite (A) and ferrite (F) from the fusion line of an austenitic stainless steel containing both phases.

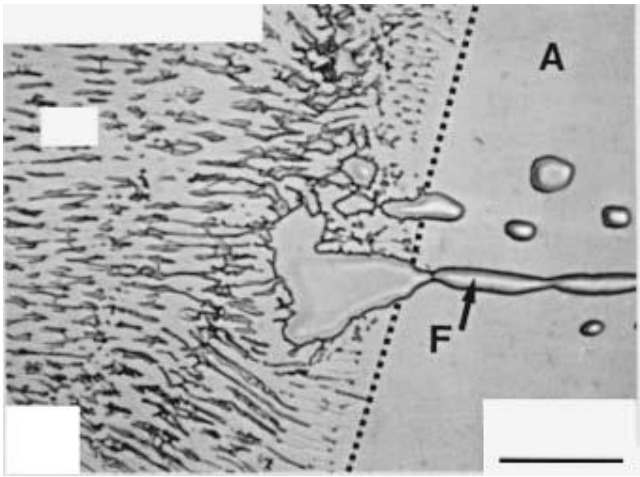

SOURCE: Elmer [51].

2.4 NICKEL BASE SUPERALLOYS

Nickel base superalloys have nickel as main element, but can also contain other important alloying features, such as chromium, molybdenum, titanium, cobalt and aluminum. The microstructure differs from polycrystalline to monocrystalline solidification. Polycrystalline solidified nickel alloys components exhibit weakness on high temperature applications. The creep strength of components depends on the grain structure, as well as the formation of pores at the grain boundaries. A method of directional solidification has been developed in which the grain boundaries are eliminated in order to improve the operation even at high operating temperatures [4]. The so-called SX superalloys prevent the appearance of pores in the structure and, therefore, are suitable for use at extremely high temperatures. These materials preserve the mechanical properties even by temperatures up to 85 % of their melting point, which distinguish them from other alloys [4]. The increasing demand for high temperature resistant materials is the main propellant for the development of such superalloys [6]. The aero engines industry makes use of this optimization of material properties in combination with thermal barrier coatings to increase the temperature in the combustion chamber, enhancing the efficiency of the engine.

The use of nickel base materials in high temperature applications is mainly limited by two points. Firstly, the melting temperature of pure nickel is 1455°C, which corresponds to applications with a maximum temperature of 1100°C. On the other hand, the thermal conductivity is relatively low and the thermal expansion coefficient is high in comparison to other alloys. At high temperatures, the thermal fatigue affects the material properties to critical levels [4].

To manufacture turbine blades, there is a need of materials with a high specific strength, excellent creep resistance and that tolerate high thermal and mechanical loads. That is the reason why nickel base superalloys are suitable for use in high-pressure turbines. Excellent creep and heat resistance properties are a result of a solid solution strengthening and precipitate formation:

Solid solution strengthening

Solid solution strengthening is achieved by the alloying of the elements: chromium, tungsten, molybdenum, cobalt, iron, titanium and tantalum. The addition of those elements introduces a deformation of the crystal lattice because of the different sized atoms integrated to the

structure. Thus, the lattice displacement is impeded, resulting in an increase of the critical shear stress [3, 54].

Precipitate formation

Some alloying elements forms with nickel a γ'-phase, which form the major part of the heat strengthening [3, 55].

2.4.1 MORPHOLOGY

Nickel base superalloys consist of two main phases: γ and γ'; the solid solution is a FCC γ-phase with precipitation of γ'-phase [56, 57]. Nickel strength is increased by alloying rhenium, molybdenum and tungsten in the γ-phase. Those elements introduce a distortion of the crystal lattice because of the different sized atoms integrated to the crystal structure. Thus, the lattice displacement is impeded, resulting in an increase of the critical shear stress [3, 54]. The γ'-phase is the fragile precipitate responsible for high thermal stability, which achieves a volume fraction up to 70 % in SX alloys. The ordered precipitates of γ'-phase are crucial for the high-temperature strength property [57]. They hinder the structure dislocation at elevated temperatures and stable the solid solution [58]. Figure 2.21 shows the typical morphology of the nickel base superalloy CMSX-4, where the γ-matrix appears as bright channels and the γ'-phase as dark rectangles. In that case, the γ'-phase is mostly formed by Ni_3Al [57].

Figure 2.21 – Morphology of single crystal nickel base superalloy CMSX-4. γ-matrix appears as bright channels and the γ'-phase as dark rectangles.

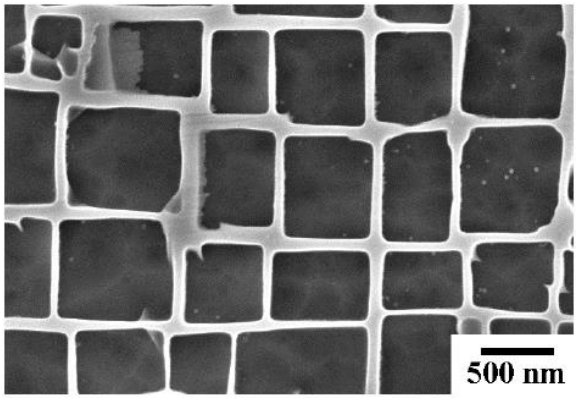

SOURCE: Göbenli [57].

The nickel base materials to be used in high temperature environments are manufactured either by conventional or powder metallurgy [59]. The conventional cast (CC – Conventionally cast) procedure results on a polycrystalline structure. However, this microstructure has poor creep and rupture strength at high temperatures and stresses. It can easily lead to grain boundary sliding and finally to intergranular material damage due to high centrifugal forces during engine operation. To reduce the grain boundary sliding along the main loading direction, alloys are developed with a directionally solidified columnar crystalline structure (DS – Directionally Solidified). DS-cast alloys consist of elongated crystals, which solidify in the direction of the main load. Thereby, most of the grain boundary sliding is avoided, which leads to an increase in the creep and rupture strength. The next improvement step is the development of a single crystalline (SX) structure. The main advantages of SX systems are the removal off all concentrated effects and damage mechanisms in the grain boundaries. These include grain boundary sliding, intergranular damage and diffusion creep. Figure 2.22 shows the different types of microstructure in a schematic representation [3, 60, 61].

Figure 2.22 – Microstructure of polycrystalline (CC), columnar crystalline (DS) and single crystal (SX) alloy.

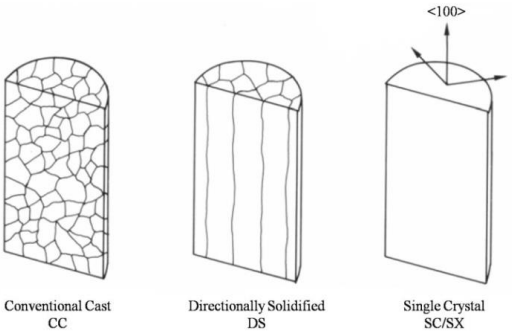

SOURCE: Brockhaus *et al*. [60].

2.4.2 PROPERTIES

From all the superalloys, the nickel based are the most widely developed concerning the mechanical, corrosive and thermal properties [62]. Nickel shows no allotropy, which is the property of some elements to exist in two or more different structural forms. The lattice structure of nickel is FCC up to the melting point, which has a lower diffusion coefficient than body-centered cubic (BCC) lattice [4].

The CMSX-4 nickel base superalloy is used in the present work. As shown in Table 2.4, it has a density of 8.7 g/cm^3 and melting temperature from 1320-1380°C. Its quasi-isotropic Young's modulus is 210 GPa at room temperature and 160 GPa at 800°C. In Table 2.5 is shown the alloying elements for the CMSX-4 composition.

Table 2.4 – Physical properties of CMSX-4.

Property	Value
Density	8.7 g/cm^3
Melting temperature	1320 – 1380°C
Young's modulus	at 20°C: 210 Gpa
	at 800°C: 160 Gpa
Thermal expansion	8.8 x 10-6/°C
Thermal conductivity	at 20°C: 11 W/m·K
	at 800°C: 22 W/m·K

SOURCE: Pollock [1].

Table 2.5 – Composition of CMSX-4.

CMSX-4 Nickel base alloy										
	Ni	Co	Cr	Ta	W	Al	Re	Ti	Mo	Hf
W_t [%]	61,7	9,0	6,5	6,5	6,0	5,6	3,0	1,0	0,6	0,1

SOURCE: Pollock [1].

For temperatures above 650°C the heat resistance of nickel alloys is even superior then from titanium alloys. In general, superalloys have low thermal conductivity due to frequent thermal cycling at high temperature peaks, which introduces stresses, cracks and there is the risk of thermal fatigue in the material. The high thermal stability is achieved by the combination of multiple mechanisms [4]. However, solid solution strengthening and precipitate formation are mainly responsible for it. Despite the high thermal stability, the material has similar ductility and fracture strains as other metallic materials. High corrosion resistance is enabled by an impermeable layer of chromium or aluminum oxide. Table 2.6 summarizes the effect of the main alloying elements over nickel base superalloys.

Table 2.6 – Effects of alloying elements over nickel base superalloy.

Element	Effect	Content up to
Cr	+ Corrosion protection + Solid solution strengthening	30 %
Co	+ Light solid solution strengthening - Reduces the phase stability	20 %
Mo	+ Increases de Young's modulus - Reduces oxidation stability	14 %
W	+ Increases de Young's modulus - Reduces oxidation stability - Increases the density	14 %
Ta	+ Formation of γ'-phase + Solid solution strengthening - Increases the densit	12 %

Al	+ + -	Formation of γ'-phase Solid solution strengthening Reduces the phase stability	6 %
Re	+ - -	Solid solution strengthening Increases the density Rare and expensive	6 %
Ti	+	Formation of γ'-phase	5 %
Hf	+ -	Reduces de hot cracking during casting Decrease the melting temperature	1,5 %

SOURCE: Durand-Charre [4].

Tensile strength

The yield and ultimate tensile strengths are relatively high for nickel base superalloys, reaching at room temperature yield strength of 900-1300 MPa and tensile strengths of 1200-1600 MPa. Figure 2.23 shows the yield strength as a function of temperature for a SX superalloy (CMSX-3) and a polycrystalline alloy (René 88 DT) [26, 45]. In the SX superalloy is possible to notice no tensile property decay until 850°C [1]. The slight rise in the yield strength of the alloy at intermediate temperatures is duo to flow of γ'-phase precipitates, as shown in Figure 2.24. This graph also adds the fact that two-phase superalloys materials are much stronger than either the matrix or the precipitate in their bulk form. The strengthening comes from multiple microstructural sources, including the solid solution strengthening, grain size strengthening and the interaction of dislocation with precipitates [64, 65].

Figure 2.23 – Variation of yield strength as a function of temperature for a SX turbine blade superalloy, CMSX-3, and a powder processed polycrystalline alloy for turbine disk applications, René 88DT.

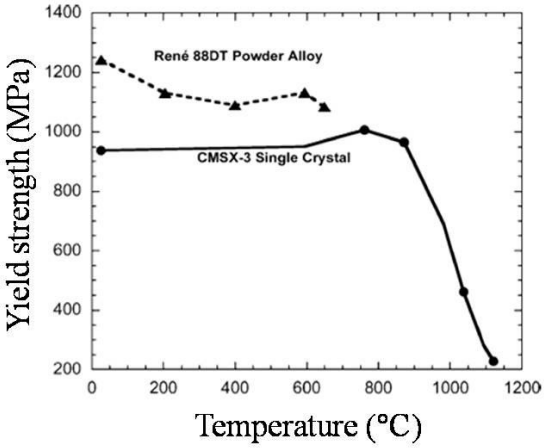

SOURCE: Pollock [1].

Figure 2.24 – Comparison of the critical resolved shear stress (CRSS) from the nickel base superalloy MAR-M200 and the individual constituent phases.

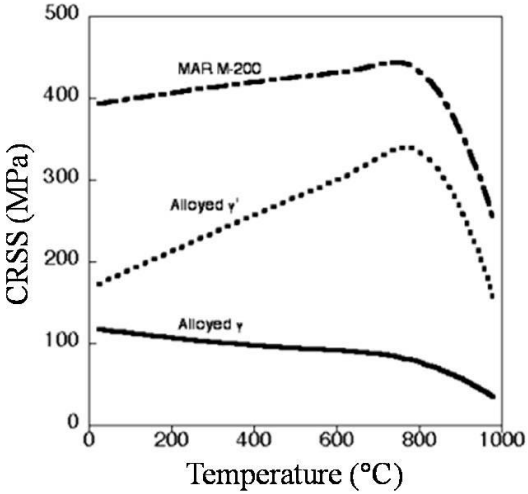

SOURCE: Loria [64].

2.4.3 TURBINE BLADES

Nickel base materials have a widespread application. In the electrical engineering field are manufactured resistance and thermocouple products. Thermal technology uses as oxidation resistant for heat conducting materials. In process and petrochemical engineering the corrosion and oxidation resistant materials are highly required [53]. A very important field of application is the manufacture of turbines blades. For the first blade rows of stationary gas turbines and aircraft engines, the use nickel base SX superalloys are increasing in comparison to CC or DS materials. The main reason is the enhancement of efficiency levels of the turbine [57].

The blade root is made in the form of tree to facilitate the mounting in the rotor, as shows Figure 2.25. The interlocking system allows a light radial movement of the blade during operation, which suppresses the vibration. It is cooled during operation by air ducts that begin in the blade root and crosses completely up to the top to withstand the high thermal loads [3].

Figure 2.25 – Typical structure of a high-pressure turbine blade.

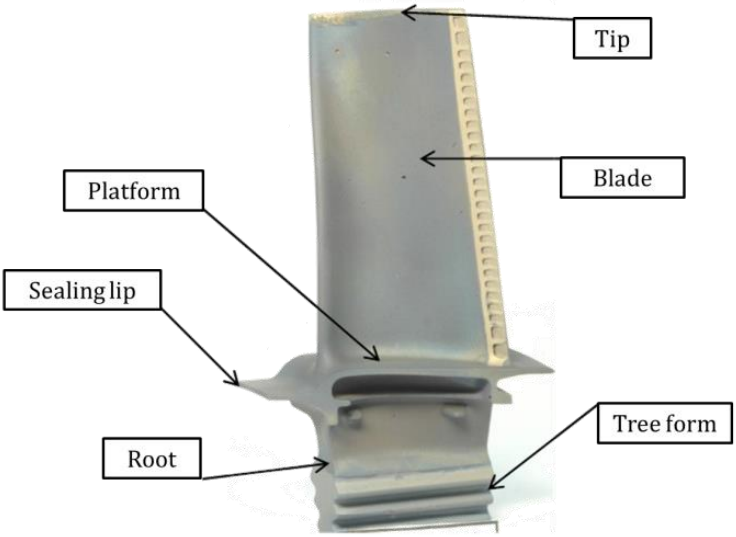

SOURCE: Weidlich [62].

The biggest challenge to cast SX structures is to define the solidification direction and avoid random crystal growth [60, 61]. The method for producing directionally solidified components most frequently used in the industry is the Bridgman-method. It is a vacuum investment casting process at 10^{-8} bar. The casting is not done in a conventional way, in which the component is cooled uniformly in all directions, but performed in a furnace to induce the solidification according to a directional heat flow [4]. Figure 2.26 shows a scheme of the process.

Figure 2.26 – Bridgman method to manufacture single crystal turbine blades.

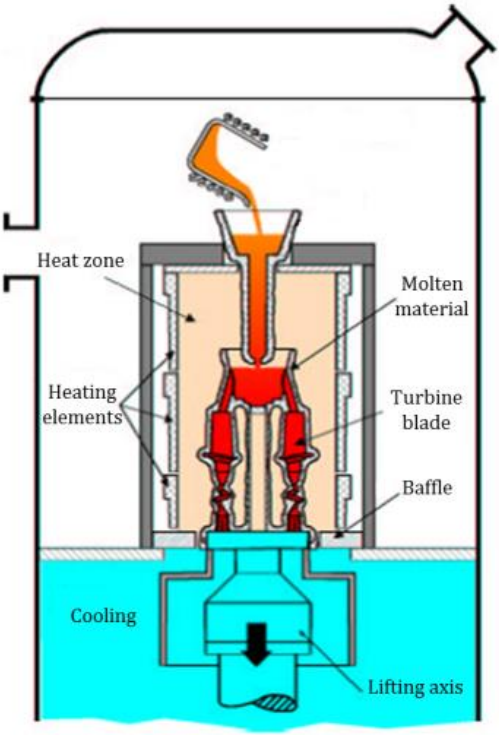

SOURCE: Steinhaus[59].

The baffle, a water-cooled copper ring, creates a temperature barrier between the furnace chamber and the lower cold region of the mold [4]. The shell mold is mounted on a water-cooled plate, which is

lowered at a defined speed to promote heat dissipation in one direction through conduction inside de component. There is also the need to avoid the growth of crystals that are not in the <001> direction, in order to achieve a SX microstructure. For this reason, the mold has at the bottom the geometry of a helix with 360 ° spiral. The continuous change of direction within the helix makes it works as a grain filter, since it permits the growth of the most favorable orientation, the <001> [4]. After the process, the turbine blade still needs a thermal treatment to uniformly distribute the generated precipitates of γ'-phase in the microstructure.

Many turbine blades also need an extra protection according to the working environment. A corrosion protection layer may be applied in order to avoid the direct contact of the base material with the hot gases present in the engine atmosphere. Without this protection, the life of the blade is highly reduced. Another protection is the addition of a thermal barrier coating, which can be an adhesive layer of ceramic. Its poor thermal conductivity protects the blade from the gas flowing around [55, 60]. Besides the coatings, the blade requires an efficient cooling, which is made by high-pressure air drawn through the blade during the operation. The blade is supplied through cooling channels in the base and the air is directed within it by air ducts. The airflow absorbers the heat from the blade walls and creates a cooling film around it [3, 60].

Despite the protection mechanisms, the turbine blades present typical damages due to high thermal and mechanical loads, such as:

Creep

Creep is one of the most usual failures in turbine blades due to continuous stress under high temperatures. It is very important for the material to be resistant to creep, due to temperatures up to 1100°C. Figure 2.27 show that, for a determined stress and temperature, the two phase γ-γ' have much higher creep resistance than their single-phase counterparts. However, there is an optimum quantity of precipitate to enhance the creep rupture life [66]. Figure 2.28 shows that point achieved by precipitate volume fractions in the range of 60-70 %, which is also the volume present in several alloys for such applications [67].

Figure 2.27 – Temperature of creep resistance by γ-γ' in comparison with their single phase.

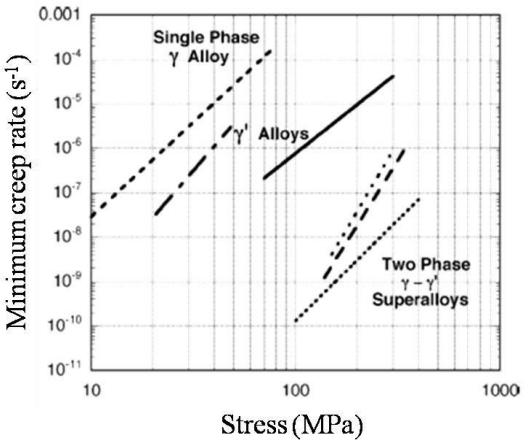

SOURCE: Pollock [1].

Figure 2.28 – Creep rupture variation as a function of γ' volume fraction for single crystal TMS-75.

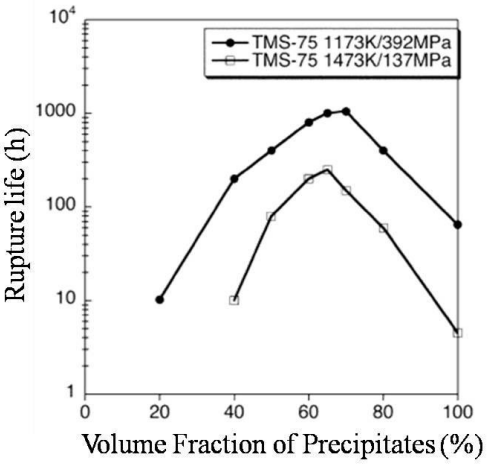

SOURCE: Murakumo *et al.* [66].

The details of deformation process are very sensitive to temperature and applied stress, which justifies the approach for creep at

low, intermediate and high temperatures. In low creep temperatures the deformation usually occurs on <110> {111} slip systems, with an initial preference for dislocation glide through the matrix. The dislocations accumulate at the γ-γ' interface and results on a shearing of the γ' precipitate. On the other hand by intermediate temperatures, stress levels are usually insufficient to shear the γ' precipitate. The deformation is mostly confined into the γ matrix. The high temperature creep enhances the diffusivity, which results in morphological changes within the microstructure [66].

Fatigue

Engine components experience significant fluctuation in stress and temperatures because of their repeated take off – cruise – landing cycles. These can introduce localized plastic strains. Fatigue properties are sensitive to mean stress, particularly at elevated temperatures. Crack initiation may occur at extrinsic inclusions that are introduced during processing or at specific microstructural such as larger grains [68]. Cast alloys may have the start of crack at porosity, as shown in Figure 2.29. Crack growth rates are sensitive to microstructural features, including grain size, precipitated sizes and volume fractions [69]. In temperatures above 500°C, environmental and cyclic aspects become significant aspects.

Figure 2.29 – Fatigue crack initiation in a pore of a single crystal superalloy.

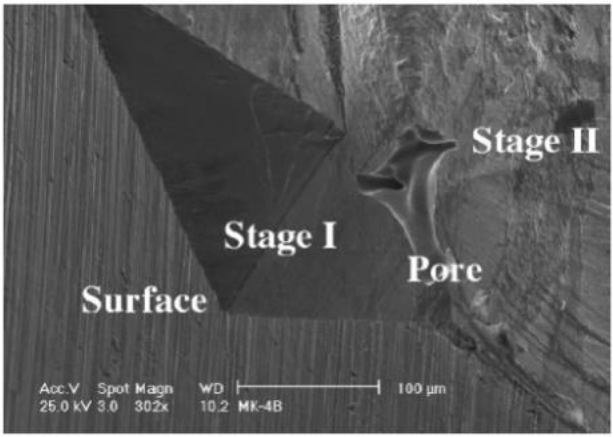

SOURCE: Pollock [1].

High temperature corrosion

The high temperature corrosion corresponds to the wear phenomena caused by hot gas in contact with the blades at temperatures above 1100°C [60]. The oxidation occurs by a chemical reaction of the atmospheric oxygen with the metal surface of the turbine blades. Inside the oxidation layer are pores and cracks that allow contact of the air molecules with the metallic surface and continue the process. The oxidation rate increases together with the temperature, which can result on a thick layer of lost material at high temperatures [3].

Erosion

The component suffers material removal from foreign particles. In engines, it often occurs due to sand and dust particles in the air [70]. Turbines that work in desert regions, for example, are adapted in order to have protection against the environmental effects on blades erosion.

3 EXPERIMENTAL SETUP

The aim of this project is the development of a laser cladding process for the repair of damaged single crystal turbine blades. The hypothesis to be proven is that wear and cracks of SX materials can be restored by laser cladding if there is introduced a temperature gradient. This gradient simulates the manufacturing process of the original part, creating a similar environment for the growth of new grains. The microstructure of the clad must have the same orientation as the original material in order to restore the part properly and keep the properties. For that, the added material must solidify in the same direction as the original microstructure.

The limitation of this process for the repair of turbine blades lies on the depth of damage, which cannot be situated in a region with cooling channels. In this case, the laser cladding is no longer suited, since it is not possible to rebuild the channels.

3.1 METHODS

The development of a maintenance method for turbine blades is approached for the two most usual damage situations, as shown in Figure 3.1. The abrasive wear is unavoidable for a turbine blade due to continuous stresses and working conditions. In order to repair the wear on the tip, the surface must be prepared for the laser cladding process. That means a flat surface without any vestige of the damaged material as, for instance, oxidation layer. However, for the cracks is needed another approach. One possibility is to remove a complete layer until the crack is eliminated, afterwards the clad may be performed. Other approach is the introduction of a notch, which reduces not only the loss by removal but also for the added material.

Figure 3.1 – Model of a damaged turbine blade.

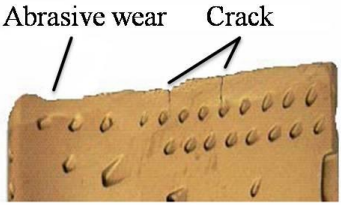

SOURCE: The author.

Figure 3.2 shows the difference between the heat flow on flat substrate and a notch. On the flat substrate, the heat flows in one direction. The clad formation inside the notch is a challenge because of the difficulties involved in the energy distribution. The heat flow tends to propagate in two dimensions, which difficult the orientation of grains during solidification. This undefined direction to grow may also introduce traction and compressions forces on the solidified material. These forces form an unstable region in which the crack and pore usually appears.

Figure 3.2 – Heat distribution on flat substrate (left) and notch (right).

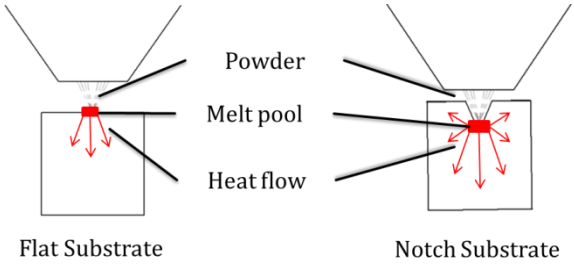

SOURCE: The author.

Due to appearance of tensile strengths on the notch, the introduction of a temperature gradient into the substrate is required to achieve a SX clad without cracks. For that, the substrate is heated up on the top, which balances superior part with higher temperatures compared to the bottom. In addition to this, a cooling unit is installed on the substrate holder for the temperature reduction on the bottom. This method reduces the tensile and compressive forces inside the notch and supports the achievement of a temperature gradient.

The experiments are carried out in order to provide knowledge about the parameters concerning the clad formation. Those are divided into three basic groups:

- Preliminary tests – parameters study
- Clad on top – clad on the top of the substrate
- Clad on notch – strategies to fulfill the notch

The preliminary tests consist of a study of the clad formation according to the variation of three basic parameters: the laser beam radius, scanning speed, cooling and laser power. They comprehend the base that is used for the application on the top and notch substrate. The goal of the top trials is to achieve a SX clad over the top, with layer upon layer. The notch difference is the geometry, which has to be fulfilled with the same microstructure as the original. Further details about each approach are described in chapter 4. A process characteristic maintained for all the experiments is the powder convergence, which is carried out on the substrate surface.

The test specimens consist of a single crystal CMSX-4 with original dimensions of 30x30x2 mm, as Figure 3.3. On the left side is represented the substrate "A", which is used for the preliminary and flat tests. On the right side, the substrate "B" piece is prepared with laser cutting for the notch experiments. In this case, each sample may be used only twice. These specimens are manufactured according to the same requirements as the turbine blade itself, which has a defined grain orientation to be followed by the new clad.

Figure 3.3 – Specimen type A and B.

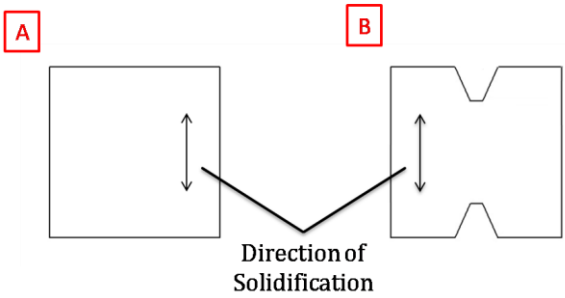

SOURCE: The author.

Figure 3.4 – Dimensions of the notch in specimen type B.

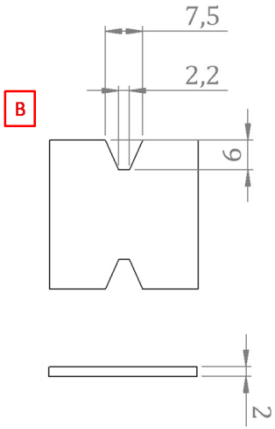

SOURCE: The author.

The test bench developed to realize the experiments consist of three components: cooling plates, inductive coil and precision elevator. The substrate is fixed in the middle of the two plates, which permits the fast heat exchange between the surfaces. Both plates have intern channels that are cooled down by cold water at 18°C. On the other side is an inductive coil, which heats up the upper part of the substrate. The elevator moves the system down in order to correct the cladding position relative to the induction coil. With this configuration is possible to achieve the temperature gradient over the substrate.

Figure 3.5 – Testing bench sketch.

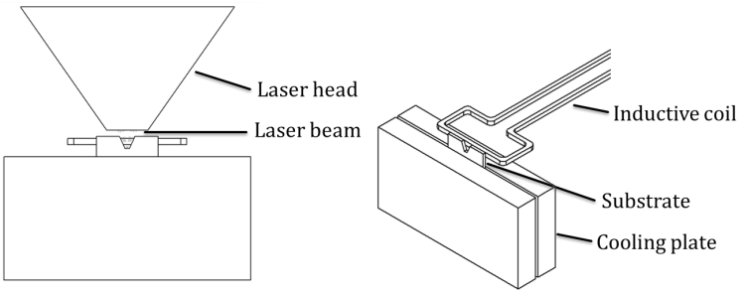

SOURCE: The author.

3.2 EQUIPMENT

The facilities from the Laser Zentrum Hannover (LZH) were used to perform almost all the experiments concerning this work. In this chapter the devices for safety, the working plant and the testing bench are described.

3.2.1 SAFETY

The use of laser equipment requires caution to avoid the injury of both operator and people on the surrounding. Everyone exposed must be advised about the risks and safety equipment, which varies according to laser type. There are two main characteristics that must be observed: class and wavelength. These properties define which gear has to be used during operation. The IEC 60825-1 [71, 72] classifies the laser source into classes from 1 to 4 (high risk) according to its hazard when in contact with humans.

The laser source used for the experiments corresponds to a class 4, which offers risks of skin burn and eye injury in case of exposal. The use of powder requires an extra care. In order to operate in safety, the equipment are (Figure 3.6):

- Lab coat – avoid powder contamination
- Gloves – avoid powder contamination
- Mask – avoid the breathing of toxic elements
- Goggle – avoid serious eye injuries.

Figure 3.6 – Safety equipment.

SOURCE: The author.

3.2.2 WORKING PLANT

"LMB automation" is an enterprise focused on the production of facilities for laser material processing. The working plant is customized according to the process type, which in this case is powder laser cladding. For that is required an enclosure to permit local exhaust ventilation due to significant quantities of powder in the air during the experiments. The monitoring may be realized by a set of cameras disposed inside or also through a small window. There are a total of five emergency switches, two outside and three inside, that disable both the axes and the laser source. Inaddition, the door has a security lock that blocks the laser usage when it is opened.

Figure 3.7 – LMB automation for laser cladding.

SOURCE: The author.

The facility is equipped with compressed air, helium, nitrogen and argon. The table used as support for the experimental equipment consists of a granite block with ca. 3 m^2, which prevent the influence of external vibrations. An adapted 6-axis milling CNC control from Siemens (Sinumeric 840D Power line with Siemens S7 300) is incorporated to the LMB. The laser head itself may be directly controlled by four from these axes (x, y, z and b), the two missing ones (a and c) are part of a testing bench. This configuration permit parts with maximum height of 800 mm and weight of 500 kg.

Laser source

The laser equipment used for the experiments is a high power diode laser LDF400-650 from Laserline. The beam is produced by four diode arrays with 5 emitters each. The light is conducted from the source to the laser head through an optical fiber. It has a continuous wave (cw), maximum power of 680 W, wavelength between λ = 940-980 nm and the beam is similar to the single mode Gaussian TEM_{00}.

The light from the optical fiber comes directly to the optical path, represented in Figure 3.8. It corresponds to a set of optical components that adjust the beam characteristics. In order to generate a parallel beam path after emerging from the optical fiber, the laser beam passes through a collimator. After it, the beam is focused by lens with focal length of 200 mm. In order to protect the optical system from process particles, there is introduced argon as shielding gas just before the lens set.

Figure 3.8 – Laser beam path through the optical components.

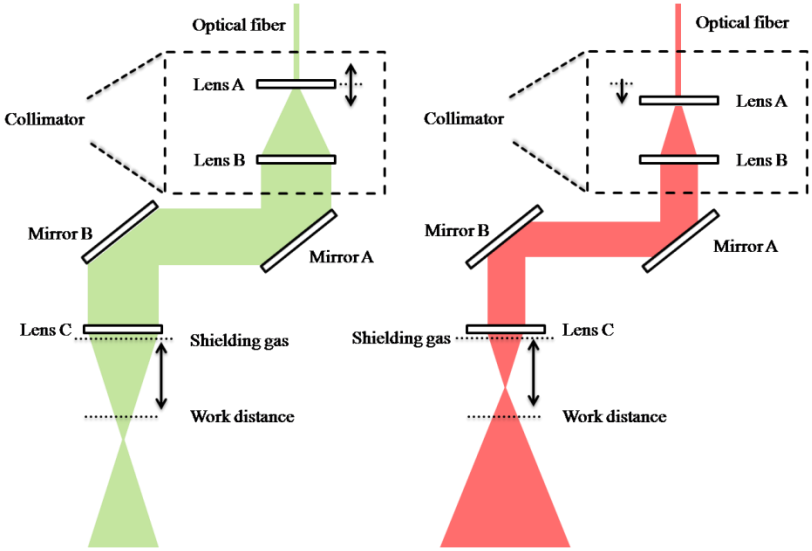

SOURCE: The author.

The set of focusing lenses has a permanently configuration. However, it is possible to change the collimator settings. This permits the laser beam to converge or diverge, according to the disposal of its

lens set. The beam is expanded at lens “A”, which are displaced along the beam axis. In Figure 3.8 is shown two examples of the collimator configuration, according to the displacement of lens “A”. The lens “B” rearranges the beam in parallel rays that are reflected through two mirrors before facing the lens “C”, which converge the beam on the focus area.

In this laser cladding process, the powder is injected into the working area with pressured argon through eight holes in the underside of the nozzle. Those powder jets convert into a point located 9 mm under the nozzle, which is the working point. The adjustment of lens “A” implicates the change of the laser focus position and consequently the beam radius in the working area. Therewith is changed the energy delivered and the beam intensity distribution, according to the beam diameter in the working surface. Regarding that, the laser focus is the region with the highest energy intensity from the laser beam. In the following are presented five configurations of the combination from laser focus and powder convergence: two before, one coincident and two after the powder convergence. The black line represents the powder convergence, the green line corresponds to the laser beam and the figure on the right is the intensity distribution on the black line.

The configurations BR1 and BR2 correspond to the laser focus above the powder convergence with beam radius of 0,992 and 0,633, respectively. In that case, part from the powder is pre-heated on the laser focus before the collision with the sample surface. BR3 has a coincident powder convergence and laser focus (radius of 0,398 mm). It is the smaller radius obtained, which transfer the higher quantity of energy into the center of the melt pool. The setup BR4 and BR5 have the laser focus under the powder convergence, and thus for a practical application the laser focus is not formed because it would be located inside the workpiece.

Figure 3.9 – Laser focus above the powder convergence (BR1).

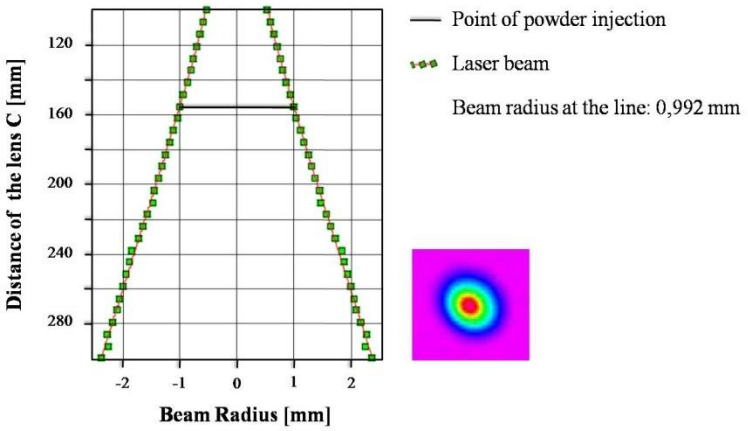

SOURCE: The author.

Figure 3.10 – Laser focus above the powder convergence (BR2).

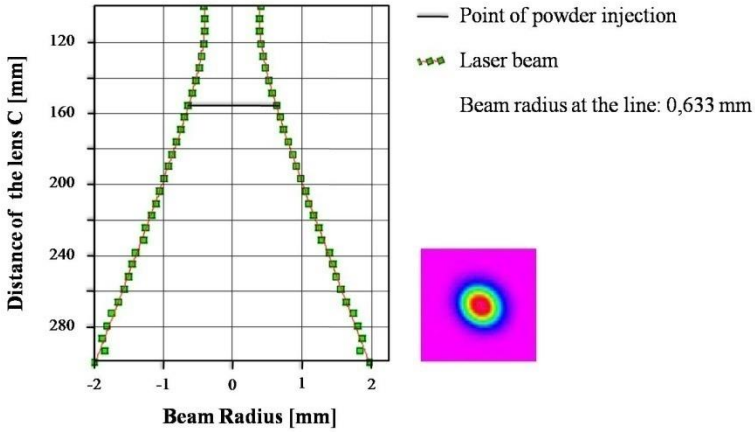

SOURCE: The author.

Figure 3.11 – Laser focus coincident with the powder convergence (BR3).

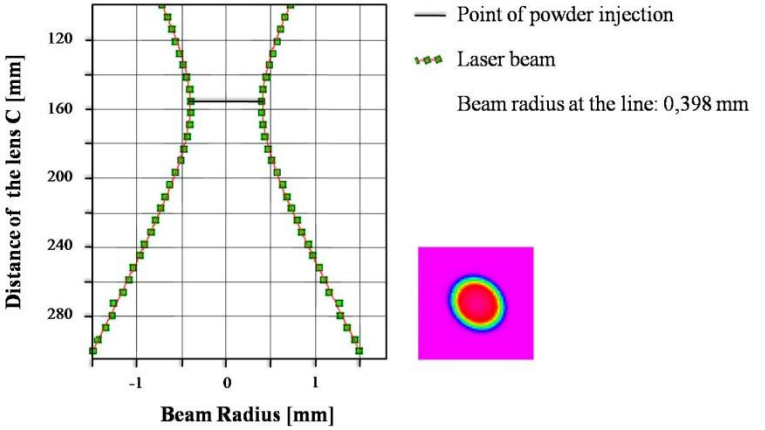

SOURCE: The author.

Figure 3.12 – Laser focus under the powder convergence (BR4).

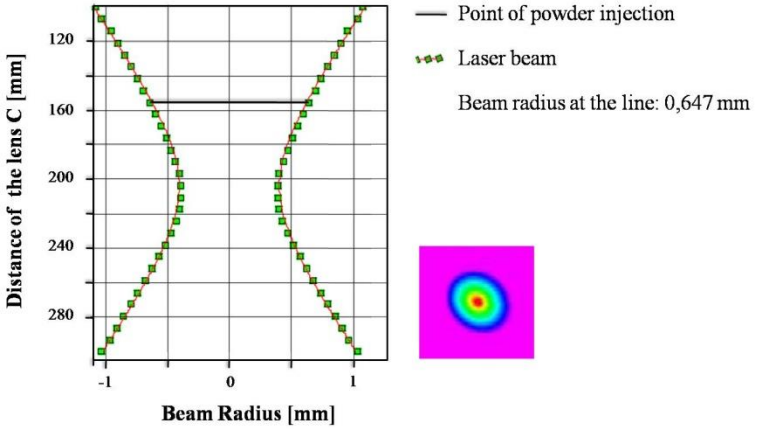

SOURCE: The author.

Figure 3.13 – Laser focus under the powder convergence (BR5).

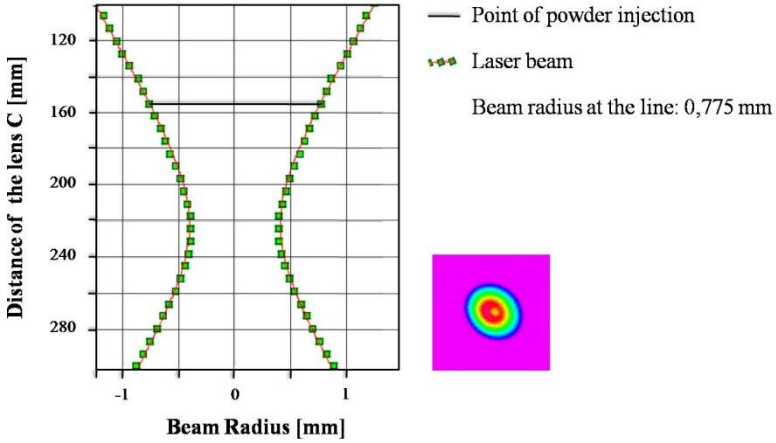

SOURCE: The author.

Besides the collimator, the laser head counts with a temperature control system. It is equipped with a Sensor Therm pyrometer (temperature range between 1000 °C and 2500 °C) for temperature reading in the same axis as the laser beam. The pyrometer combined with a PID control system (TemCom) permits the laser power to be balanced according to the desired temperature in the melt pool.

Powder feeder

The powder feeder is the GTV Twin 2/2, which has gravity as operational principle (type B from Table 2.2) and two chambers for storage up to three liters. These chambers are pressurized with argon, which guides the particles and form an oxidation free atmosphere. The powder stands under pressure and is forced to fill in the disk slot. The support of gas flow guarantees exact and reproducible powder feed rate. Thereby powder feed rate is linearly proportional to the feeder disc rotation. There is also a stirrer inside to keep the powder constantly in circulation and prevent the feeder obstruction by generation of conglomerates inside de chamber.

Figure 3.14 – Powder feeder GTV twin 2/2.

SOURCE: The author.

The disk rotation is controlled by a Siemens TP170 system located in the front part of the feeder or directly by the machine CNC control. Each powder requires a calibration to estipulate the quantity of powder dispatched to the process, which depends mostly on the material density, powder size and gas pressure.

3.2.3 TESTING BENCH

The testing bench is enclosed by acrylic walls, except at the top, to avoid the powder dispersion and keep the shielding gas inside the chamber. In addition to this is a local exhaustion unit to remove the flying particles. There are three main devices used inside the acrylic chamber: induction coil, precision elevator and cooling system. Figure 3.15 shows the disposal of those devices.

Figure 3.15 – Testing bench.

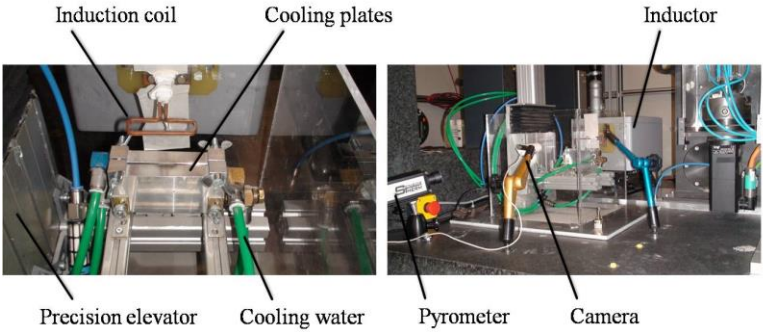

SOURCE: The author.

The thermal induction device is an IEW – TTH3 (G/H) with 3 kW of maximum power, in which a copper coil is used to preheat the substrate. The substrate cooling is performed by two aluminum plates cooled down with water at 18°C. A precision elevator is used during the process to maintain the working area at a determined distance from the induction coil. Surrounding is an acrylic box that does not permit the powder to spread all over and keep the shielding gas inside the chamber. The substrate is fixed between the cooling plates, near enough to the induction coil to be heated up.

3.3 ANALYSIS

Approach to the powder analysis of the material used for the experiments in order to certificate the composition and the shape of grain powder. For the specimen evaluation there are two methods described.

3.3.1 POWDER

The nickel alloy CMSX-4, described in chapter 2.3, has to be sieved and analyzed to certificate its grain size and composition. The importance of such investigation lies on the reproducibility of process parameters, allowing the consistency of studies.

Sieve

The sieve has to be located in an isolated area with exhaust ventilation, since many materials are harmful and requires a proper breathing mask for the people in this atmosphere. The device has four main parts, but it is possible to use several sequential sieves as shown in Figure 3.16.

Figure 3.16 – RetschVibrotronic VE1.

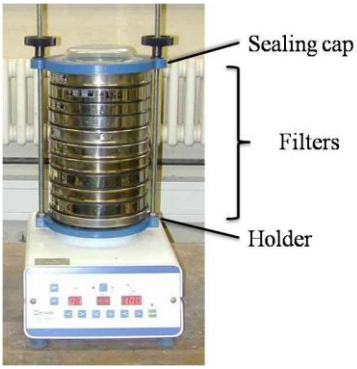

SOURCE: The author.

It operates with a motor on the bottom responsible for vibrating the entire system in order to promote the circulation of particles. The powder is added into the first sieve, which has the bigger mesh. As the motor starts, the smaller particles tend to fall into the next recipient until reach the holder at the bottom. At the end, the grains are separated according to the mesh of the sieves.

The powder used for the experiments are supposed to have grain diameter between 25 and 75 µm, although there are cases of mismatch, for bigger and smaller ones. That requires the sieving of every powder used, once there could be found grains under and over the size described for the manufacturer. The investigation consists of a sample analyzed in a scanning electron microscope. The upper part of Figure 3.17 shows the powder after the first sieving, which still has particles under 25 µm. The presence of such small parts can generate discontinuity on the structure due to bonding problems with the bigger particles. Because of that, a second sieving to separate the small particles from the powder is needed. This time the powder size was raised to the range between 25 and 100 µm. Moreover, the time and vibration were increased to force the conglomerates to disperse. The bottom part of Figure 3.17 shows the result after the second sieving. The increase of the vibration amplitude and operation time could eliminate the residual particles of the first sieving.

Figure 3.17 – Powder analysis.

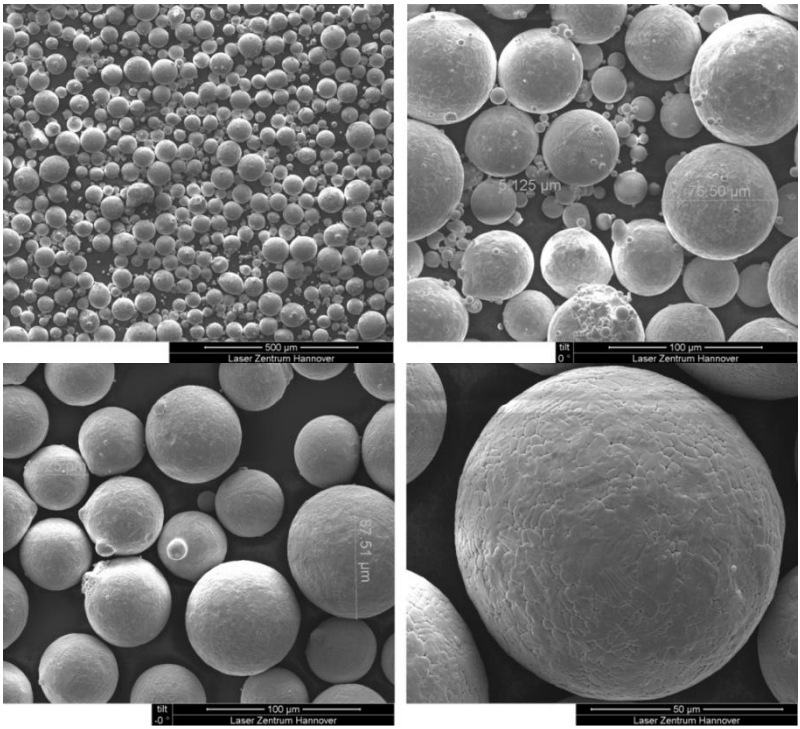

SOURCE: The author.

Composition

The EDX method is a dispersive X-ray spectroscopy to evaluate the material composition. It is an analytical technique for the elemental analysis or chemical characterization that relies on the material excitation with X-ray radiation for the generation of a spectrum. Each element has a unique atomic structure and generates a set of peaks, thus can be defined its quantity. The X-Ray spectrum of the CMSX-4 is shown in Figure 3.18.

Figure 3.18 – EDX analysis.

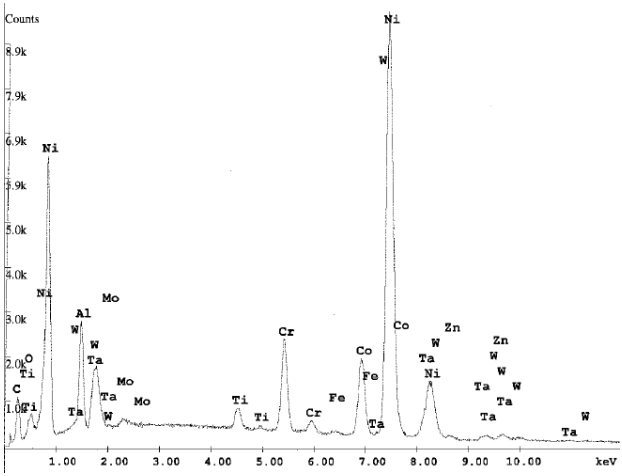

SOURCE: The author.

The Table 3.1 shows the material weight percentage found in the literature according to Pollock [1] and the analysis of CMSX-4 used for this work. The elements of this nickel base superalloy alloy are cobalt, chrome, tantalum, tungsten, aluminum, rhenium, titanium, molybdenum and hafnium. The alloy composition investigated in the lab test is in accordance with the literature. Despite a difference of 7.8 % for cobalt and 6.7 % for tungsten, all the significant elements have exact the same percentage.

Table 3.1 – CMSX-4 composition.

CMSX-4 Nickel alloy [w_t%]										
	Ni	Co	Cr	Ta	W	Al	Re	Ti	Mo	Hf
Literature	61,7	9,0	6,5	6,5	6,0	5,6	3,0	1,0	0,6	0,1
Analysis	60,6	9,7	6,5	6,5	6,4	5,6	3,0	1,0	0,6	0,1

SOURCE: Pollock [1].

3.3.2 SPECIMEN

The specimen analysis is necessary to verify the microstructure of the clad after the process. That way is possible to testify the absence of crack and pores as well as the formation of a single crystal

microstructure. The samples may be analyzed by two methods: metallography and EBSD. The institute (LZH) has a surface analysis laboratory capable of metallography evaluation, which speeds up the results.

Metallography

Metallography is the microscopic study of the structure of metals and their alloys. Material surfaces and fractures are examination can reveal valuable information as to the crystalline chemical, and mechanical heterogeneity. The crystalline heterogeneity is known metallographically as grain. Chemical heterogeneities comes from impurities, segregation of chemical elements, and nonmetallic inclusions. Mechanical heterogeneity consists of local deformation of structure, elongation or distortion of nonmetallic inclusions, and regions of chemical segregation, resulting from cold fabrication process. The surface must be polished or etched in order to reveal the size and shape of grains, distribution of structural phases, microsegregation and others structural conditions [73].

Metallography is the prior method applied to study the structure of the specimen used in the experiments. It enables the verification of pores and cracks, which are the usual problems found on the clad as shown on the left of Figure 3.19. Another important characteristic is to have a good estimation about the solidified orientation, as shown on the right of Figure 3.19.

Figure 3.19 – Crack and pore detection by metallography analysis.

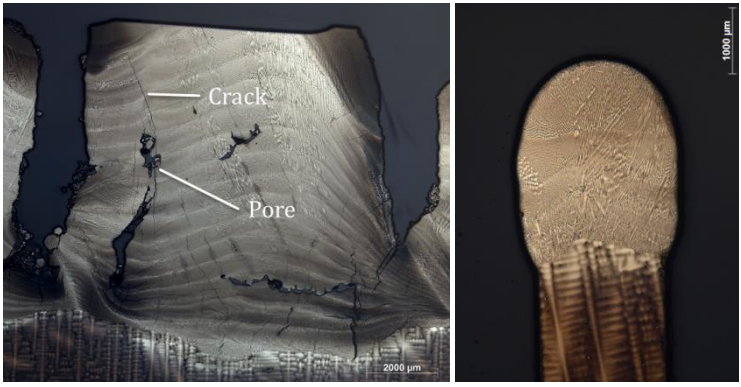

SOURCE: The author.

EBSD

Electron BackScatter Diffraction (EBSD) is a relatively new, scanning electron microscope-based technique used to characterize microstructures and textures in crystalline metal and ceramic materials. Accelerated electrons of a SEM are diffracted by atomic layers, which can be detected when they collide on a phosphor screen generating visible lines (Figure 3.20). These projections correspond to patterns of the geometry of the lattice planes in the crystal, which enables the evaluation of the crystalline structure and crystallographic orientation.

Figure 3.20 – Electron Backscatter Diffraction setup.

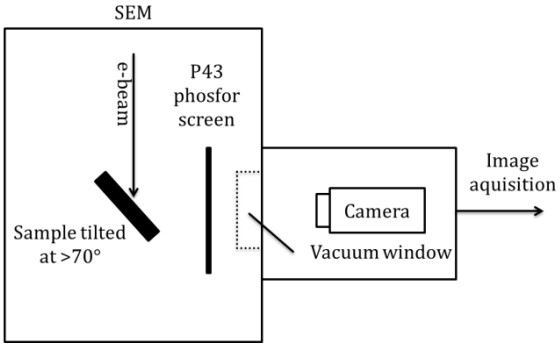

SOURCE: Swapp [74].

Figure 3.21 shows a sample submitted to metallography (left) and EBSD (right). On the EBSD is possible to observe a pattern of a SX microstructure in yellow that corresponds to the sample in the bottom and the clad on the upper part. The same region of the metallography has also a pattern where the grain growth explicit in the same direction of the original sample microstructure. This comparison between both analysis techniques permits a prior evaluation of the clad microstructure by metallography.

Figure 3.21 – Metallography (left) and EBSD (right).

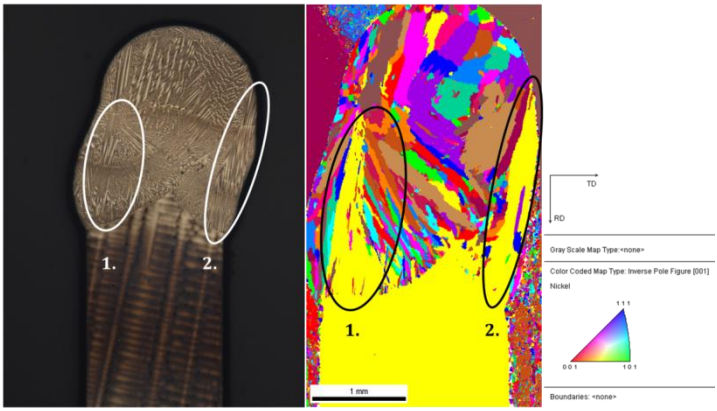

SOURCE: The author.

4 EXPERIMENTAL RESULTS

The experiments were carried out in the facilities of the Laser Zentrum Hannover, with the equipments described in section 3.2. There are three groups of analysis: preliminary tests, clad on top and clad on notch. The parameters used for each experiment are exposed in tables, which present the following abbreviations:

- SA Sample
- BR Beam Radius
- SS Scanning Speed
- CD Cooling Distance
- LI Laser Beam Intensity
- PD Powder Quantity
- PH Pre-heating
- TE Temperature
- NT Notch

4.1 PRELIMINARY TESTS

In order to have a parameter study about the clad formation and the mechanisms involved, the preliminary tests present an approach of the beam radius on the substrate, scanning speed, cooling and laser beam intensity. They constitute a base that is used for the further experiments (flat and notch substrate). In the first experiment (beam radius), the preheating is applied. However, in the next three it is removed in order to avoid any kind of influence on the clad formation. Figure 4.1 illustrates the path used for the laser head to clad on the substrate, which consists on a 6 mm length line repeated five times. The height adjustment between each clad is realized by the elevator.

Figure 4.1 – Cladding strategy.

SOURCE: The author.

A typical form of the clad formation in these trials is shown in Figure 4.2; however in this example were performed 15 tracks to facilitate its observation. It is to be noticed that according to the advance, from the left to the right, the clad height decreases. This happens due to highly increase of temperature during the processes, reaching at the end the level in which the layers are melt and the wall is unmade.

Figure 4.2 – Typical clad form.

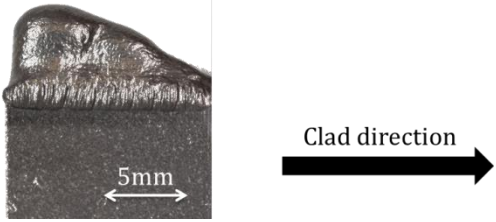

SOURCE: The author.

4.1.1 BEAM RADIUS

The laser beam focus may be changed according to the collimator settings, as detailed in the chapter 3.2.2. There are three basic laser focus configurations: above, coincident, and after the powder convergence. It is important to highlight that the beam radius considerate for the experiments is actually the beam radius on the working surface, not necessary on the laser focus. Table 4.1 shows the parameters used for the experiments.

Table 4.1 – Process parameters for the beam radius variation.

SA	BR [mm]	SS [mm/min]	CD [mm]	LI [W/cm^2]	PD [g/min]	PH [°C]
BR1	0,992	100	7	$0,5 \cdot 10^4$	3	650
BR2	0,633	100	7	$1,9 \cdot 10^4$	3	650
BR3	0,396	100	7	$7,7 \cdot 10^4$	3	650
BR4	0,671	100	7	$1,9 \cdot 10^4$	3	650
BR5	0,775	100	7	$1,0 \cdot 10^4$	3	650

SOURCE: The author.

Samples BR1 and BR2 have the laser focus above the powder convergence and beam radius on the substrate surface of 0,992 mm and 0,633, respectively. The powder melt before reaching the surface generates a wider clad, but there is no grain orientation near the surface and much of the material was lost to the lateral. Samples BR4 and BR5 have the laser focus under the powder convergence, which means that the laser is not formed. Since the powder convergence is localized on the substrate surface, there is no physical space for the laser beam to focus. This configuration results on a beam radius on the surface of 0,671 mm and 0,775, respectively. The configuration BR3 is the only one with a coincident powder convergence and laser focus, which has on the surface a beam radius of 0,396 mm. This setup provides the highest power intensity available of 77000 W/cm^2.

The metallography of those five samples is shown in Table 4.2. It is possible to observe not only the quantity of melted powder, but also how it melted on the surface. The first impression given by those pictures is that BR1 and BR2 have more melted powder than the others. A fact not confirmed by the Powder Usage Ratio (PUR), which calculates the percentage of used powder that was actually bonded to the surface. Those results are presented in Table 4.3. It occurs because the metallography was made in a random position on the clad, which has not the same height in its complete length as presented in Figure 4.2.

According to Bruck [43], the melt pool must have the smallest depth possible in order to obtain a layer with less diluted material. It is not possible to measure the dilution levels of those experiments due to reference loss during the process. However, BR3 and BR4 present a more homogeneous dilution over the surface. In addition to this, BR3 has also shown the required grain orientation near the surface and the best PUR.

Table 4.2 – Metallography evaluation of the beam radius variation.

BR1 (0,992 mm)	**BR2 (0,663 mm)**
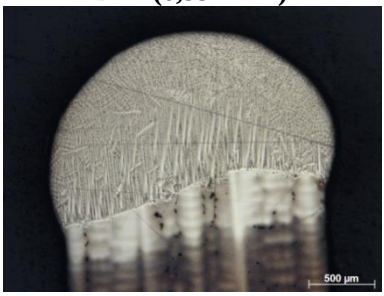	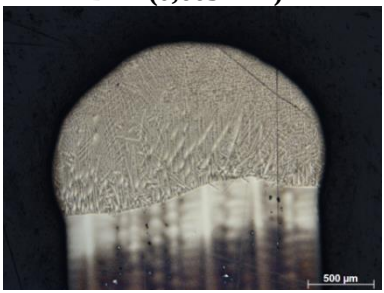
BR3 (0,396 mm)	**BR4 (0,671 mm)**
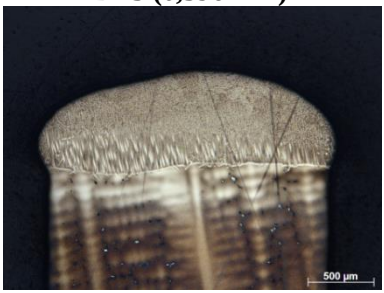	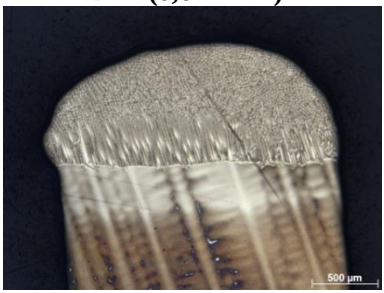
BR5 (0,671 mm)	
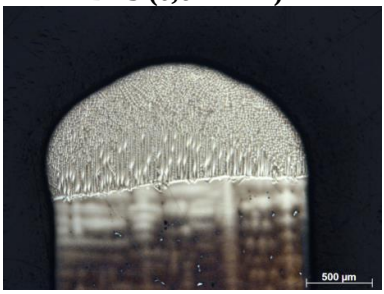	

SOURCE: The author.

Table 4.3 – Powder Usage Ratio for the beam radius experiments (PUR).

SA	PUR [%]
BR1	20,8
BR2	27,5
BR3	29,2
BR4	20,0
BR5	26,7

SOURCE: The author.

4.1.2 SCANNING SPEED

Scanning speed is an expression imported from cutting processes (feed rate) that means the speed at which the cutter is fed against the workpiece. For laser cladding it represents the speed of the laser head, which influences the quantity of powder and energy delivered per area. The working plant has linear motors that provide scanning speeds up to 4000 mm/min. Although for most powder injection applications such speed is not needed. The experiments evaluate the process behavior under four different scanning speeds: 50, 100, 150 and 200 mm/min. The parameters used are shown in Table 4.4.

Table 4.4 – Process parameters for the scanning speed variation.

SA	BR [mm]	SS [mm/min]	CD [mm]	LI [W/cm^2]	PD [g/min]	PH [°C]
SS1	0,396	50	4	$6{,}2 \cdot 10^4$	3	-
SS2	0,396	100	4	$6{,}2 \cdot 10^4$	3	-
SS3	0,396	150	4	$6{,}2 \cdot 10^4$	3	-
SS4	0,396	200	4	$6{,}2 \cdot 10^4$	3	-

SOURCE: The author.

Table 4.5 shows the metallography results for the scanning speed variation experiments. Unlike the results obtained with the beam radius, there are remarkable differences between the specimens. According to Lugscheider *et al.* [34], the scanning speed varies the amount of powder and energy delivered to the sample. It changes the molten bath temperature and consequently the quantity of powder melted down, as presented in Table 4.6 by the fact that PUR values are reduced as the

speed increases. According to Gedda [36], the dilution levels are higher by the increase of energy in the melt pool. In Table 4.5, is possible to observe the reduction of dilution levels as the scanning speed increases, which occurs because the same power intensity is applied with different exposal time.

In SS1, it is possible to observe the larger clad, since the low scanning speed has an influence on the quantity of energy delivered to the melt pool. However, he dilution level is the highest obtained and the solidification is not epitaxial near the fusion zone. From the four samples, SS2 and SS3 have shown the better microstructure. In both cases is to notice a homogeneous clad with low dilution.

The PUR values are inferior in comparison with the results from the focus trials. This effect is justified by the absence of preheating in the experiments, which reduces the quantity of powder added to the surface and results on a smaller clad.

Table 4.5 – Metallography evaluation of scanning speed variation.

SS1 (50 mm/min)	**SS2 (100 mm/min)**
	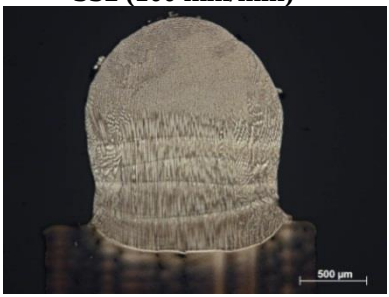
SS3 (150 mm/min)	**SS4 (200 mm/min)**
	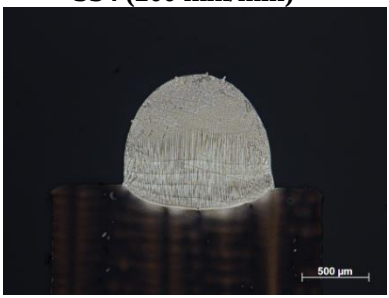

SOURCE: The author.

Table 4.6 – Powder Usage Ratio Powder for the scanning speed experiments (PUR).

SA	PUR [%]
SS1	12,3
SS2	9,9
SS3	9,4
SS4	8,6

SOURCE: The author.

4.1.3 COOLING DISTANCE

The cooling is a point of relevance for the generation of a temperature gradient. It is performed directly by the sample holder, which is made of two aluminum plates cooled down with water. The specimen is fixed by these two plates allowing the heat change as Figure 4.3 shows.

Figure 4.3 – Cooling unit.

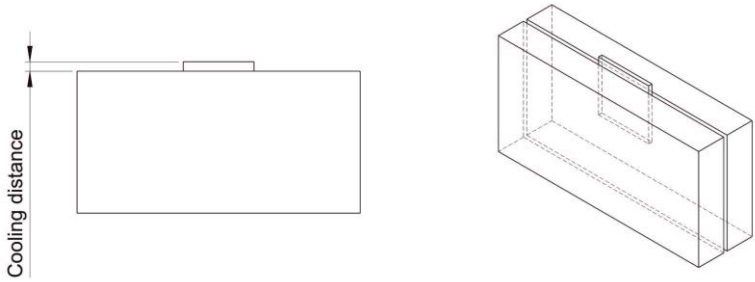

SOURCE: The author.

There are two manners to improve the directed thermal gradient: water temperature and the distance from the cooling plates. The water is cooled down by the main chiller, which is maintained always at 18°C. However, the distance between the substrate surface and the plates can be adjusted. Therefore experiments varying the distance from 2 to 7 mm are performed in order to introduce different temperature gradients in the substrate. In addition, Table 4.7 shows that for every distance was evaluated two different power intensities: 62000 and 123000 W/cm^2, respectively.

Table 4.7 – Process parameters for the cooling distance variation.

SA	BR [mm]	SS [mm/min]	CD [mm]	LI [W/cm^2]	PD [g/min]	PH [°C]
CD1	0,396	100	2	$6{,}2 \cdot 10^4$	3	-
CD2	0,396	100	3	$6{,}2 \cdot 10^4$	3	-
CD3	0,396	100	4	$6{,}2 \cdot 10^4$	3	-
CD4	0,396	100	5	$6{,}2 \cdot 10^4$	3	-
CD5	0,396	100	6	$6{,}2 \cdot 10^4$	3	-
CD6	0,396	100	7	$6{,}2 \cdot 10^4$	3	-
CD7	0,396	100	2	$12{,}3 \cdot 10^4$	3	-
CD8	0,396	100	3	$12{,}3 \cdot 10^4$	3	-
CD9	0,396	100	4	$12{,}3 \cdot 10^4$	3	-
CD10	0,396	100	5	$12{,}3 \cdot 10^4$	3	-
CD11	0,396	100	6	$12{,}3 \cdot 10^4$	3	-
CD12	0,396	100	7	$12{,}3 \cdot 10^4$	3	-

SOURCE: The author.

In Table 4.8 and Table 4.9 are presented the metallography results of the cooling experiments. It is possible to notice the epitaxial solidification and its correlation with the distance from the cooling plate. For both power intensities, the clad present similar characteristics to the respective distances. However, it is important to notice that the clad width expand according to the power intensity increase, which justifies the wider clad in the samples from Table 4.9.

Despite the differences observed on the energy levels, the metallography analysis may be realized independent from the laser power, distinguishing it just by the cooling distance. In the samples CD5, CD6, CD11 and CD12, with 6 and 7 mm respectively, is important to observe that the distance influenced the clad formation, resulting on non-directed grain growth. The samples CD1, CD2, CD6 and CD7, with 2 and 3 mm from the cooling plate, present more homogeneous growth until the top of the clad than the samples previously mentioned. The problem to work with such small distances is that it makes impossible to add the preheating on the top, once most of the heat is lost directly to the cooling unit. Finally, the samples with distances of 4 and 5 mm are situated on a point that still allows the usage of preheating by induction and achieve the SX orientation as shown in samples CD3, CD4, CD9 and CD10.

According to Turnbull [49], the energy barrier ΔG for the crystal to nucleate on the substrate will decrease with the increase of undercooling. For the experiments, the smaller the distance between substrate surface and cooling plate, the higher the undercooling. This explains the better results observed for the smaller distances. For that reason further experiments are made with a distance of 4 mm, in order to improve the temperature gradient and permit a the epitaxial solidification. The distance to the cooling plates barely influence the PUR results. The difference is highlighted with the increase of energy, as shown in Table 4.10.

Table 4.8 – Metallography evaluation of cooling variation – I (6200 W/cm2).

CD1 (2 mm)	**CD2 (3 mm)**
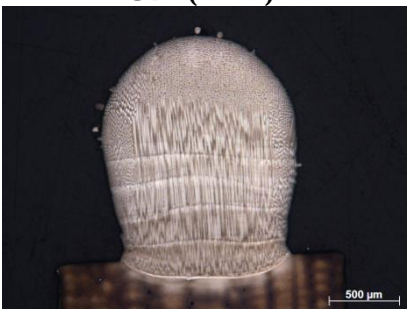	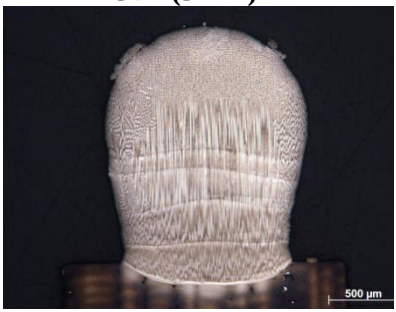
CD3 (4 mm)	**CD4 (5 mm)**
	
CL5 (6 mm)	**CL6 (7 mm)**
	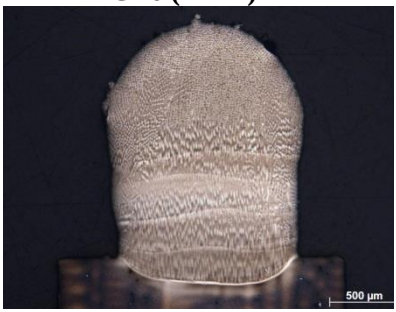

SOURCE: The author.

Table 4.9 – Metallography evaluation of cooling variation – II (12300 W/cm2).

CD7 (2 mm)	CD8 (3 mm)
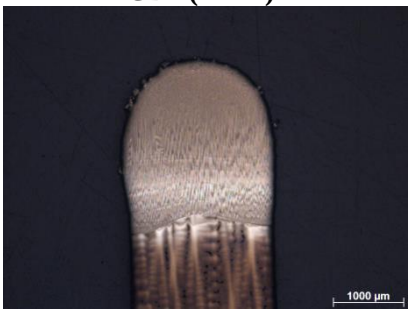	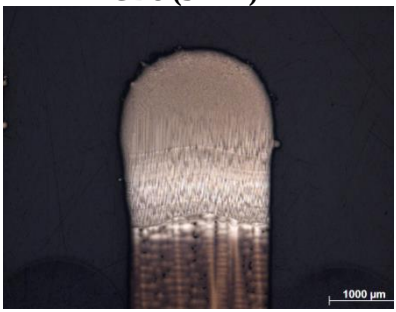
CD9 (4 mm)	**CD10 (5 mm)**
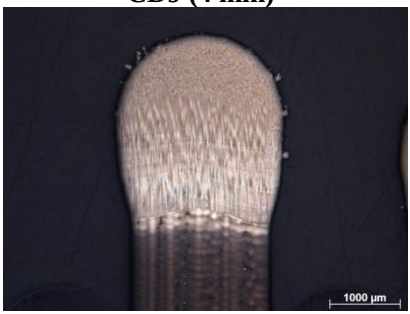	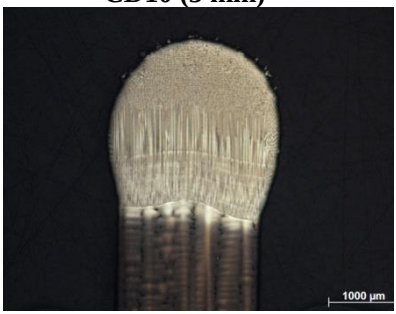
CD11 (6 mm)	**CD12 (7 mm)**
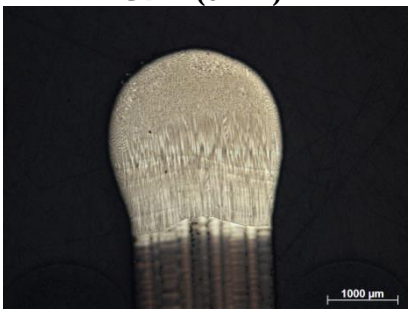	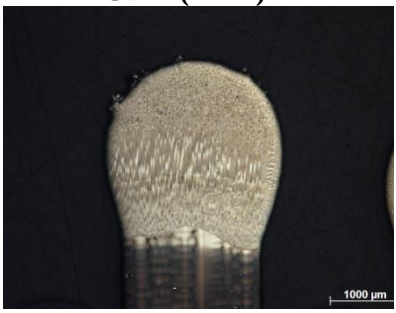

SOURCE: The author.

Table 4.10 – Powder Usage Ratio for the cooling experiments (PUR).

SA	PUR [%]
CD1	9,1
CD2	10,0
CD3	10,4
CD4	12,0
CD5	9,6
CD6	11,7
CD7	17,3
CD8	19,0
CD9	20,1
CD10	18,4
CD11	19,3
CD12	18,9

SOURCE: The author.

4.1.4 LASER BEAM INTENSITY

According to Kaierle [11], the laser beam intensity is defined by equation (3), where P_L is the laser power and A_L the laser beam profile (area). It represents the energy delivered to a defined area. The experiments were carried out in order to evaluate the clad formation under five different laser intensities, as shown in Table 4.11.

Table 4.11 – Process parameters for the laser power variation.

SA	BR [mm]	SS [mm/min]	CD [mm]	LI [W/cm^2]	PD [g/min]	PH [°C]
LI1	0,396	100	4	$6{,}2 \cdot 10^4$	3	-
LI2	0,396	100	4	$7{,}7 \cdot 10^4$	3	-
LI3	0,396	100	4	$9{,}2 \cdot 10^4$	3	-
LI4	0,396	100	4	$10{,}8 \cdot 10^4$	3	-
LI5	0,396	100	4	$12{,}3 \cdot 10^4$	3	-

SOURCE: The author.

In Table 4.12 is shown the metallography from LI1 to LI5, according to the increase of the beam intensity in the process. The quantity of melted powder on the surface is the more noticeable change in the clad formation, which may be testified by the PUR values in

Table 4.13. The modification on the clad formation occurs due to increase of energy, which also enhance the melt pool temperature and quantity of melted substrate and higher material dilution. According to Kou [41], higher levels of dilution may degrade the substrate. The amount of energy delivered affects the substrate and can even condemn the sample. That is not the case of those five samples analyzed; however, it should be considerate for the utilization of higher beam intensities.

Another aspect to be noticed is the clad width, which turns from a concave lateral form on LI1 to a convex in LI5. The clad should be neither concave, due to lack of material, nor convex, because the extra material hardly present epitaxial solidification. A control of the energy amount is needed in order to avoid such clad form.

Table 4.12 – Metallography evaluation of laser beam intensity.

LI1 (62000 W/cm^2)	LI2 (77000 W/cm^2)
	
LI3 (92000 W/cm^2)	**LI4 (108000 W/cm^2)**
	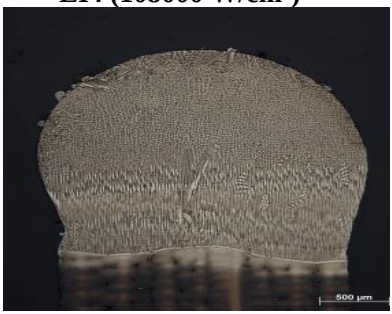
LI5 (123000 W/cm^2)	
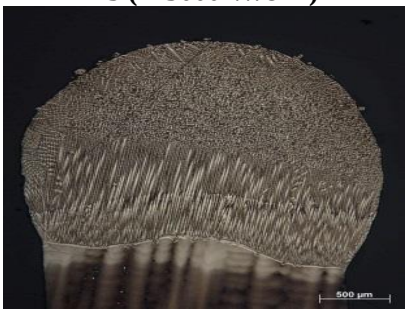	

SOURCE: The author.

Table 4.13 –Powder Usage Ratio (PUR).

Sample	PUR [%]
LI1	10,2
LI2	11,7
LI3	15,4
LI4	16,7
LI5	17,2

SOURCE: The author.

4.1.5 CLAD ANALYSIS

Independent of the modified parameter, the results of metallography in the primary tests have presented a common characteristic on the top of every specimen. In this area is noticed a different solidification pattern if compared with the bottom, where the temperature gradient is higher. In Figure 4.4 is represented the metallography and strategy used on the preliminary tests (left) and an additional experiment (right). On the left is possible to identify the five enumerated clad layers and after that, the respective area appears. On the right side is presented a clad with the same process parameters, but 10 track instead of 5. The comparison of both show a similar clad formation and the area on the top is kept. A possible reason is that the laser beam diameter is much smaller than the powder convergence focus. The melt pool starts to solidify just after the passage of the laser beam, but there is still powder ricocheting in this pool. The lack of energy in the melt pool reduces the temperature gradient and an epitaxial solidification is no longer possible. A possible solution for this problem is to repeat the path without powder, just with the laser radiation, in order to remelt and solidify it again.

Despite the undesirable formation of a region on the top, which corresponds to equiaxed solidification, the method is still valid. There is the need of removal of the last layer to repair this kind of defect. However, a finishing process is required after the cladding in any case.

Figure 4.4 – Metallography evaluation of the last cladding track.

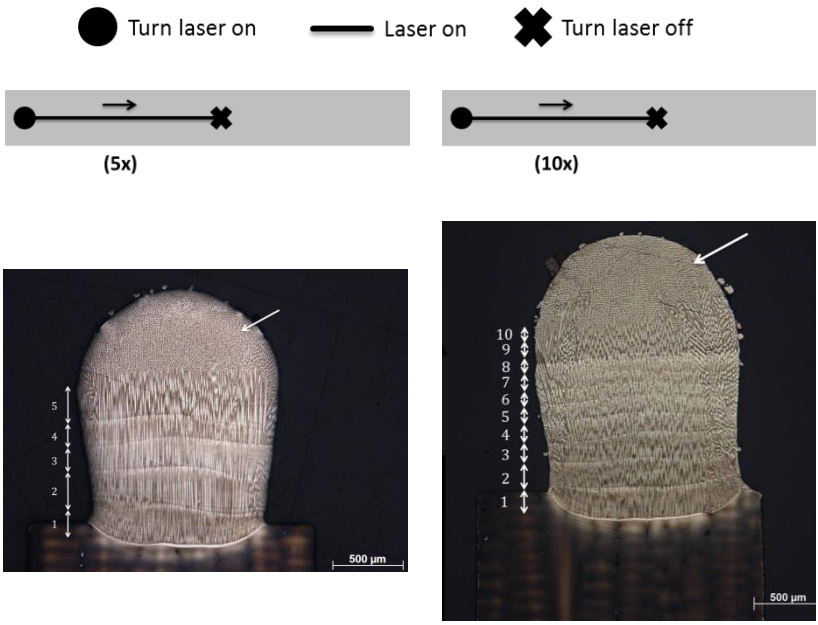

SOURCE: The author.

4.2 CLAD ON TOP

The clad on the top of the substrate corresponds to the second battery of experiments. The main idea is to develop a method to execute a clad on the entire surface, which may be applied to repair the abrasive wear on the tip of damaged turbine blades. For this goal three groups of experiments are performed: strategy, temperature and powder. The objective for the first group is to achieve a reliable strategy to clad the top of the substrate. The second evaluates different melt pool temperatures to define which the ideal energy amount to perform a stable process. The last group varies the behavior of the previous parameters with other quantities of powder. The general goal is to achieve a homogeneous clad with SX microstructure and, if possible, higher PUR to reduce the cost.

4.2.1 CLAD STRATEGY

The preliminary tests were useful to comprehend the clad formation according to the change of fundamental parameters. Although the strategy used has to be improved in order to achieve a homogeneous clad. For that were tested five ways to perform the same type of clad on the substrate (S2, S3, S4, S5 and S6), presented in Figure 4.5. In addition to this, the laser beam intensity is controlled in order to maintain the same melt pool temperature during the process.

The adapted 6-axis milling CNC control from Siemens executes just one program line at a time. It can be a problem for laser applications because of the process characteristics. In the strategy S1, for example, the command line is: move x-axis / turn laser on / move x-axis. There is a quick stop between each program line, which is enough to build up powder over the surface. That effect cause an instable clad formation, at least for small lengths.

The strategies S2, S3, S4 and S5 were performed to eliminate the effects of turning the laser on and off over the surface. These four strategies are performed on half of the substrate length in order to find out a strategy able to use one sample for more than one experiment. The strategies S3 and S4 present the better results in comparison with S1, S2 and S5. However, those five methods are still unsuitable due to the instability during the clad formation. The solution for that is S6, which uses one substrate for each parameter and clad the entire top of it. A positive characteristic of this strategy is the direct use for the clad on top purpose of cladding in the entire substrate surface. The strategy S6 is used as standard for all the clad on top experiments.

Figure 4.5 – Clad strategies.

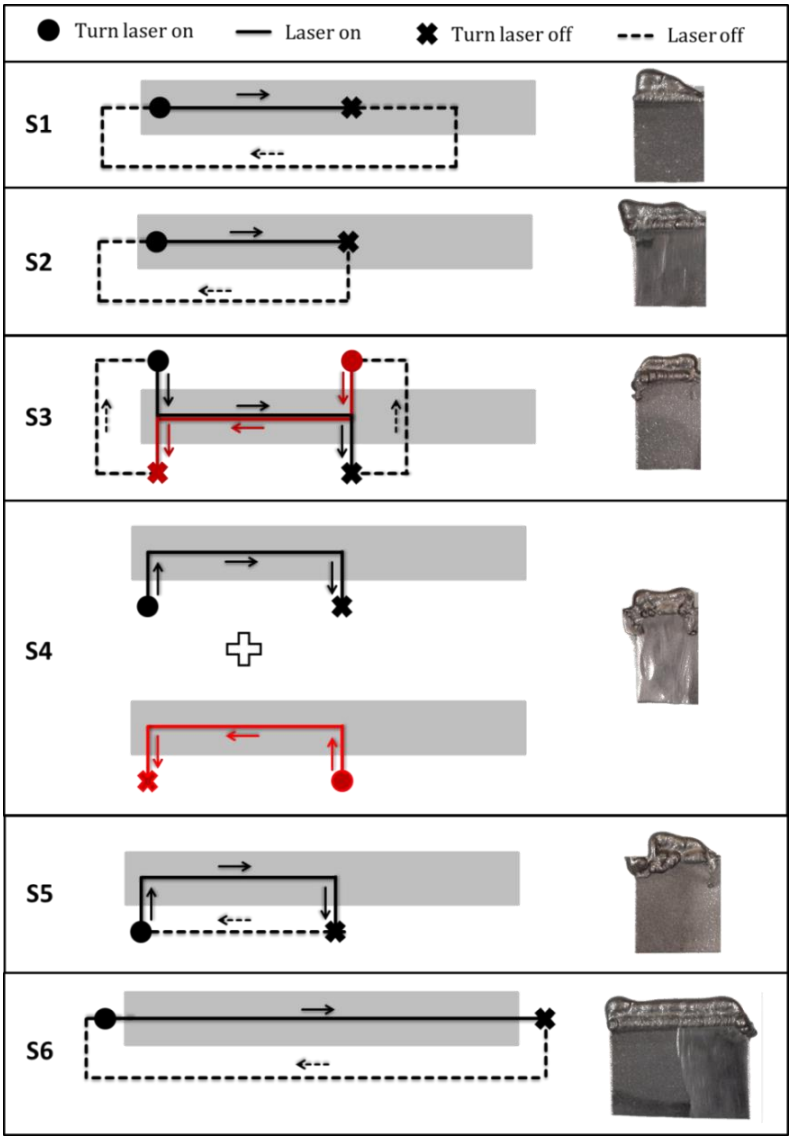

SOURCE: The author.

4.2.2 TEMPERATURE

In the preliminary tests, the melt pool temperature varied during the process, according to the amount of energy delivered. However, this may lead to high dilution levels according to Kou [41]. In extreme situations, previous layers are affected and the microstructure is compromised. In order to stabilize the clad formation, a control system is implemented to adjust the laser beam intensity according to the temperature. A pyrometer is installed in the same axis of the laser beam and is capable to read the temperatures from 1000 to 2500°C. This data is processed by a PID program that emits a signal to the laser source to compensate the temperature deviation. It is possible to set the desired temperature in the melt pool and the maximum and minimum laser power to be used.

According to the material manufacturer, the melting point of CMSX-4 is reached between 1320 and 1380°C. For the trials were selected three temperatures near the melting point: 1350, 1400 and 1450°C. Table 4.14 shows the process parameters for this group.

Table 4.14 – Process parameters for the melt pool temperature variation.

SA	BR [mm]	SS [mm/min]	CD [mm]	TE [°C]	PD [g/min]	PH [°C]
TE1	0,396	100	4	1350	3	-
TE2	0,396	100	4	1400	3	-
TE3	0,396	100	4	1450	3	-

SOURCE: The author.

The use of a control system to set a defined temperature on the melt pool, instead of a defined laser power, caused a good impact for the clad formation. It avoided the under- and overheating of the powder and substrate. Table 4.15 shows the metallography results TE1, TE2 and TE3 in a cross section (left) and a longitudinal cut (right). The three temperatures were able to achieve a clad with epitaxial solidification without pores or cracks. In the longitudinal cut is possible to observe a homogenous clad over the entire surface, corresponding to the ten layers built. The use of 1400°C melt pool temperature presents the better clad due to SX microstructure.

Table 4.15 – Metallography evaluation of temperature variation.

TE1 (1350°C)	
	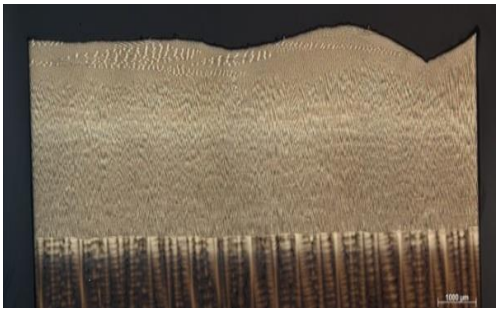
TE2 (1400°C)	
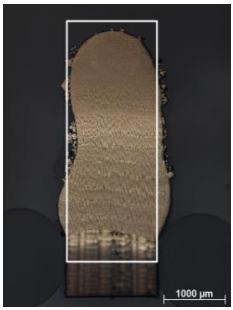	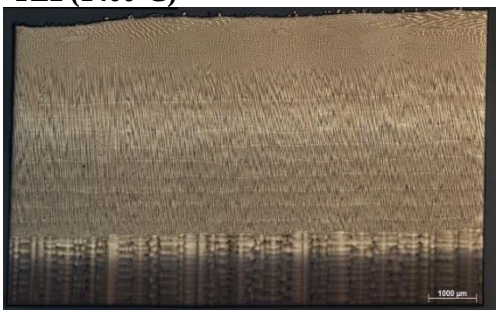
TE3 (1450°C)	
	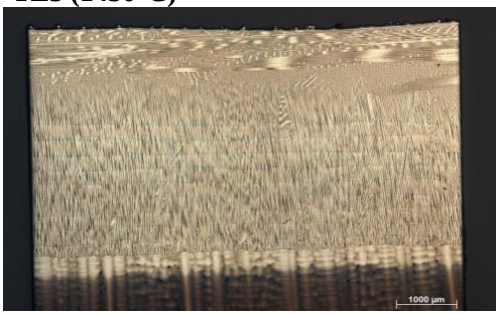

SOURCE: The author.

According to Turnbull [49], the nucleation occurs in the substrate grains at the fusion line. Since the liquid metal of the weld pool is in contact with these grains and wet them completely, there are no difficulties for the nucleation from the liquid metal upon the substrate grains. In the experiments evaluated, a homogeneous solidification occurs from the fusion line to the top of the sample. On the other hand, the cross section reveals an asymmetric formation due to lateral loss of material, which present lack of material. The clad width must comprehend at least the thickness of the substrate, in order to be considered a valuable repair. Further experiments are needed in order to refine the clad and fulfill those regions.

Table 4.16 – Powder Usage Ratio for the temperature experiments (PUR).

SA	PUR [%]
TE1	14,8
TE2	19,3
TE3	19,6

SOURCE: The author.

4.2.3 POWDER

The previous experiments have already shown a homogeneous and successful process to clad the top of the substrate. Currently, the main idea is to optimize this clad formation by correcting the lateral material loss. For that, the parameter TE2 is used as standard to test two other powder quantities: 2 and 4 g/min, as shown in Table 4.17.

Table 4.17 – Process parameters for the powder feed rate variation.

SA	BR [mm]	SS [mm/min]	CD [mm]	TE [°C]	PD [g/min]	PH [°C]
PD1	0,396	100	4	1400	2	-
PD2	0,396	100	4	1400	4	-

SOURCE: The author.

The Scanning speed (v) and the powder quantity (m) influences the geometry of the clad layer. Cladding thickness depends on the amount of material given to the melt pool during the process. It is usual

to combine both parameters to define the powder feed rate as *m/v* [g/min], to calculate the amount of powder added to the process per unit time [34, 35]. This influence can be noticed in Table 4.18, in which both parameters present a different geometry. However, the powder reduction in PD1 from 3 to 2 g/min has shown the better results. In the longitudinal cut is possible to observe the maintenance of the epitaxial solidification without pores and cracks. In addition to this, the correction of the lateral deviance is achieved, which is confirmed by the cross sectional figure on the left.

Table 4.18 – Metallography evaluation of powder variation.

	PD1 (2 g/min)
	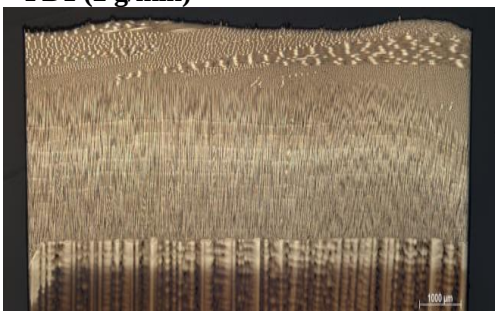
	PD2 (4 g/min)
	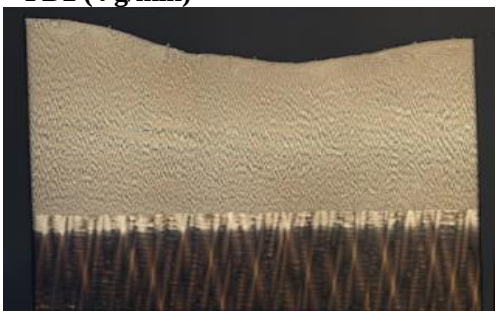

SOURCE: The author.

Table 4.19 – Powder Usage Ratio for powder experiments (PUR).

SA	PUR [%]
PD1	17,5
PD2	19,1

SOURCE: The author.

4.2.4 CLAD ANALYSIS

The results obtained with PD1 on the powder experiments have shown all the characteristics necessary to be evaluated as single crystal. For that reason, the sample was submitted to an EBSD analysis. On the left of Figure 4.6 are presented regions where misorientations were detected, which are explicit on the right with a color scale. The misorientation angle is less than 4 degrees for 40 % of the detected region and over 65 % corresponds to an angle smaller than 15 degrees, as presented in Table 4.20.

According to Turnbull [49], if the crystal crosses the energy barrier ΔG the possibility to nucleate is imminent. The presence of a temperature gradient during the experiments induces the epitaxial grain solidification. However, it is possible that at some point of the process, an unexpected energy deviation in the melt pool weaken the main solidification direction. This change could cause the misorientation observed in Figure 2.16. Another possibility is the nucleation of some grains during the sample fabrication by cutting from larger dimensions into the 30x30 mm. Both machining as laser cutting may cause temperature elevation to promote the cutting, which enables the formation of new grains in the fusion line.

The results have shown an oriented microstructure without cracks or pores, which can be verified by the EBSD analysis. Despite the misorientations, the technique may be implemented and optimized on the tip of turbine blades.

Figure 4.6 – PD1 EBSD analysis.

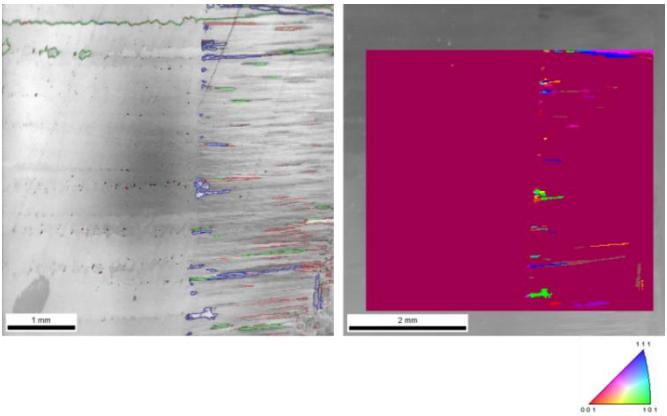

SOURCE: The author.

Table 4.20 – Misorientation angle.

Angle (degrees)	Percentage [%]	Angle (degrees)	Percentage [%]
4	40	**35**	3
7	14	**38**	2
10	7	**41**	1
13	6	**45**	2
16	2	**48**	3
19	6	**51**	2
22	2	**54**	1
26	2	**57**	2
29	2	**60**	1
32	3	**63**	0

SOURCE: The author.

4.3 CLAD ON NOTCH

The clad on the notch refers to the third group of experiments, which are exposed several strategies used to fulfill the groove introduced. The notch must be weldable in order to promote the solidification in the same oriented plane as the original microstructure. For that, a thermal induction is introduced to reduce the temperature gradient in the lateral region of the notch. With this is expected to keep

the substrate epitaxial direction as the main orientation for the new grains, as shown in Figure 4.7. The induction coil is placed 2 mm away from the substrate to preheat the top, while the bottom is cooled down continuously. This method creates a region less suitable for residual stresses inside the fulfilled notch because of the temperature homogeneity, which is also a manner to prevent cracks. The idea behind this method is to proportionate a heat flow similar to the observed in the clad on top (chapter 4.2), as shown in Figure 4.8.

Figure 4.7 – Methodolgy applied to reduce the temperature gradient in the lateral of the notch.

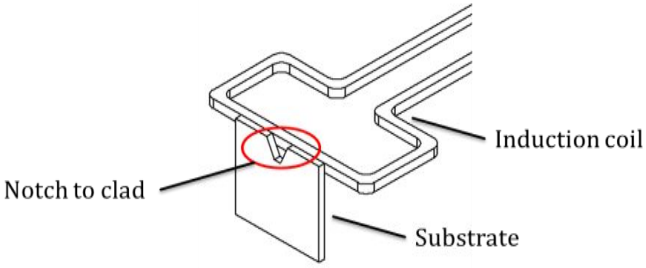

SOURCE: The author.

Figure 4.8 – Energy distribution inside the notch without (left) and with preheating (right).

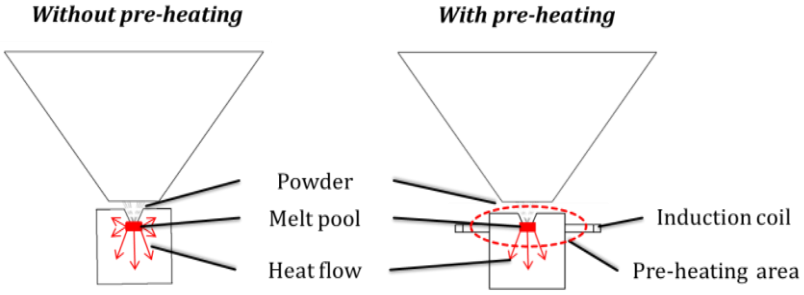

SOURCE: The author.

4.3.1 PARAMETER

The parameter study performed on chapters 4.1 and 4.2 are used as basis for the clad on notch experiments The strategy used to perform the experiments is adapted to fulfill the notch completely. For that, instead of one single track, there is used a multi-layer technique as shown in Figure 4.9, with three tracks side by side. The clad is done through two cladding directions, one beginning from the left and the other from the right, in order to build up a symmetric clad. Beyond is added an increment on the lateral component between each clad in order to compensate the notch geometry according to the clad growth. After each clad the precision elevator operates to correct the working surface height, according to the new layer, so that it remains in the same working position. In order to avoid overheating, the process starts on the same side as the induction coil due to higher temperature.

Figure 4.9 – Strategy to clad the notch.

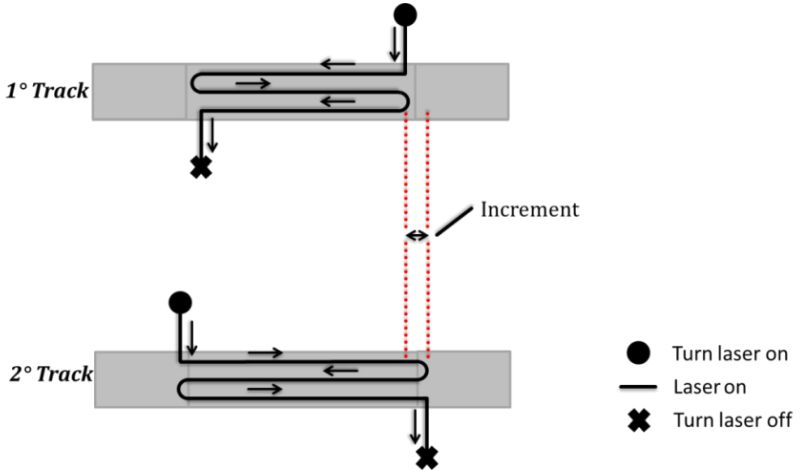

SOURCE: The author.

The first trial corresponds to a replication of the parameter TE2 from chapter 4.2.2, which achieved the epitaxial solidification on the clad. It is executed and repeated with and without the preheating to evaluate its influence on the clad formation, as presented in Table 4.21.

Table 4.21 – Process parameters for the notch fulfilment – I.

SA	BR [mm]	SS [mm/min]	CD [mm]	TE [°C]	PD [g/min]	PH [°C; W]
NT1	0,396	100	4	1400	3	-
NT2	0,396	100	4	1400	3	2000; 650
NT3	0,396	100	4	1400	3	-
NT4	0,396	100	4	1400	3	2000; 650

SOURCE: The author.

The metallography results are presented in Table 4.22, which corresponds to the longitudinal cut of each specimen. The two first samples correspond to the clad without (NT1) and with preheating (NT2). The microstructure of NT1 approximates to the SX solidification, but there are cracks and pores on it. On the other hand, NT2 shows a crack free clad with equiaxed solidification. Since the preheating is the only difference between both, it is reasonable to assume that the microstructure is vulnerable to the thermal induction influence. In order to reinforce the assumption, the parameters are repeated in NT3 and NT4. However, this time the clad is fulfilled and then is performed a clad on the top, with the same conditions as in the previous experiments. In the longitudinal cuts is possible to observe that it presents the same characteristics as NT1 and NT2. The cross sectional cuts is shown the part correspondent to the clad on top, which verifies similar results to the chapter 4.2 for the sample without preheating.

Table 4.22 – Metallography evaluation of notch fulfilment – I.

NT1	**NT2**
	
NT3 (Longitudinal)	**NT4 (Longitudinal)**
	
NT3 (Cross section)	**NT4 (Cross section)**
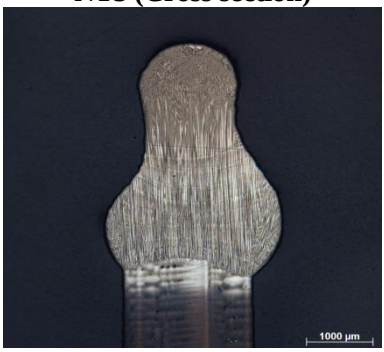	

SOURCE: The author.

These four samples show clearly that the preheating has a strong influence on the grain growth during solidification. This fact is approached with more details in the chapter 0, where the magnetic field is evaluated. For the moment is important to consider that the thermal induction, despite providing a crack free microstructure, is unsuitable for the formation of a single crystal clad. However, both trials without the preheating have shown cracks, which are also unacceptable.

According to Gedda [36], a linear relation exists between the powder feed rate and the energy required, if sufficient energy is available to melt all arriving powder. Xiangling *et al.* [42] sates that the added material is exposed to compressive stress and that in HAZ is under tensile stress. Compressive stress at the surface is favorable, but tensile stresses result in premature failure. Those stresses can be adjusted by controlling the scanning speed of the laser beam over the substrate. The following step is a parameter change to pursue the formation of thinner layers in order to reduce the temperature loss to the sides and thus avoid the residual stress. These parameters are presented in Table 4.23. In the two first samples, NT5 and NT6, there is a reduction of the powder injection. In NT7, the scanning speed is increased by 50%. The specimen NT8 corresponds to a larger beam radius of 0,671 mm to spread the powder more homogeneously on the surface.

Table 4.23 – Process parameters for the notch fulfilment – II.

SA	BR [mm]	SS [mm/min]	CD [mm]	TE [°C]	PD [g/min]	PH [°C; W]
NT5	0,396	100	4	1400	2	-
NT6	0,396	100	4	1400	1	-
NT7	0,396	150	4	1400	3	-
NT8	0,671	100	4	1400	3	-

SOURCE: The author.

As shown in the metallography results from Table 4.24, thinner layers could be achieved in specimens NT5 and NT6. However, it is not efficient to avoid the crack formation. This damage may be linked with the energy distribution on the clad (Figure 4.8).

Table 4.24 – Metallography evaluation of notch fulfilment – II.

NT5	NT6
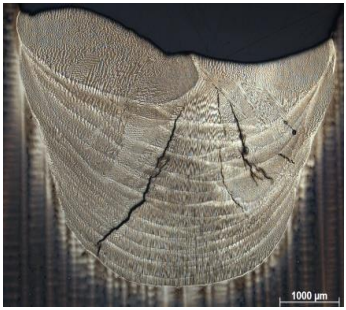	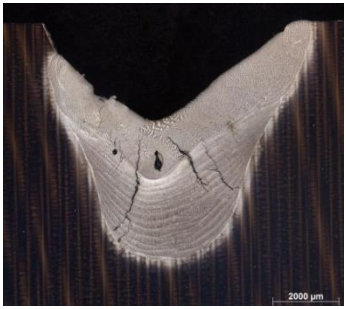
NT7	**NT8**
	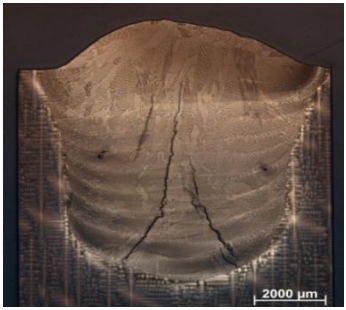

SOURCE: The author.

4.3.2 CLAD STRATEGY

With the results from the parameter study, it is possible to conclude that substrate preheating is needed to stabilize the upper region and prevent the residual stress. For the experiments is necessary to achieve a clad strategy in order to maintain the SX structure and avoid the cracks. For that, there is used the same base of parameters (Table 4.25), but with different strategy to use the thermal induction in order avoid the polycrystalline microstructure, as shown in Table 4.26.

Table 4.25 – Process parameters for the notch fulfilment – III.

SA	BR [mm]	SS [mm/min]	CD [mm]	TE [°C]	PD [g/min]	PH [°C;W]
NT9	0,396	100	4	1400	3	2000; 500
NT10	0,396	100	4	1400	3	2000; 650
NT11	0,396	100	4	1400	3	2000; 650
NT12	0,396	100	-	1400	3	2000; 650
NT13	0,396	100	-	1400	3	-
NT14	0,396	100	-	-	3	-

SOURCE: The author.

Table 4.26 – Notch strategies.

Sample	Strategy	Objective
NT9	The induction is set distant 5 mm from the substrate, instead of 2 mm	Reduce the magnetic field influence on the substrate.
NT10	The induction preheats the substrate and is shut down just after each clad	Remove the magnetic field influence during solidification
NT11	The induction preheats the substrate and is shut down just before each clad	Remove the magnetic field influence during the cladding and solidification
NT12	The induction preheats the substrate and is shut down just before each clad.	Reduction of the temperature gradient maintain a higher preheating during the clad
NT13	Without preheating. Reduced cooling	Reduction of the temperature gradient
NT14	Without preheating and temperature control. Reduced cooling	Removal controlled systems

SOURCE: The author.

Table 4.27 presents the metallographic results according to the strategies described. The sample NT9 is the outcome of a weaker preheating during the process. It is possible to notice that the influence from the thermal induction is reduced as the analysis shows the initial formation of a single-crystal microstructure in the bottom region. In order to reduce even more the action of the thermal induction, NT10 and NT11 are samples in which it is shut down after and before the clad, respectively. In NT10, where the device is turned off after the clad is not efficient due the high cooling and fast solidification, which resulted in a polycrystalline microstructure. However, NT11 shows an improvement in the microstructure since there is no magnetic field acting during the process.

In the experiments NT12, NT13 and NT14 the substrate is fixed in a support, which is placed over the cooling plates. This avoids the direct cooling, reducing the temperature gradient involved in the process. The objective is to preheat the substrate and keep higher temperatures during the clad. This reduces the energy loss to the lateral region from the notch and induces the solidification in the desired epitaxial direction. In experiment NT12, it was possible to keep the preheating for longer time before it is completely cooled down, as expected. However, the results still present cracks. In the specimen NT13 the cladding without the preheating and reduced cooling. The single-crystal microstructure is achieved for the most part of the clad, but there are cracks on the upper left region. The last sample was realized with a different strategy to achieve the molten bath temperature. The first two tracks were performed with 92300 W/cm^2 and then 10800 W/cm^2 is used. It presents a crack free clad with SX and polycrystalline microstructure.

Table 4.27 – Metallography evaluation of notch fulfilment – III.

NT9	NT10
	
NT11	**NT12**
	
NT13	**NT14**
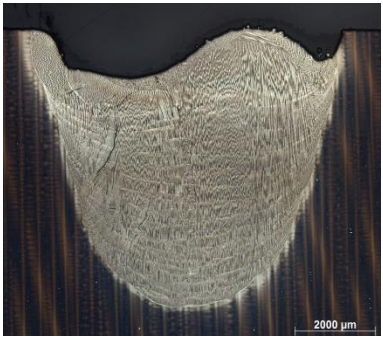	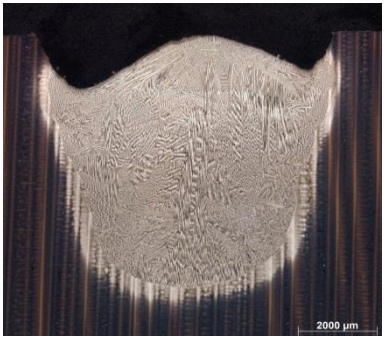

SOURCE: The author.

4.3.3 CLAD ANALYSIS

In this chapter, the crack formation and the preheating influence for the clad on notch is evaluated.

Crack formation

Neither the preliminary tests nor the clad on top have shown cracks; however, the persevering formation of cracks on the notch cladding is an important fact to be analyzed. It is clear that the notch geometry turns the SX clad into a complex system due to heat distribution and residual stresses in the region.

Lugscheider *et al.* [34] assert that for larger areas by laying single tracks next to each other, the overlap of tracks is considered another process parameter. Too small tracks results on a poor clad formation. The increase of overlap the surface becomes smoother, but every track produces a heat treatment in the preceding track. Between two overlapping tracks, a heat-affected zone (HAZ) is developed in the clad layer [36]. According to Xiangling *et al.* [42], the coating material is exposed to compressive stress and that in HAZ is under tensile stress. Compressive stress at the surface is favorable, but tensile stresses result in premature failure.

The crack is analyzed with a SEM in order to evaluate and discover its origin. On the left of Figure 4.10 is shown a sample with a crack marked by a red circle, which is detailed in Figure 4.11 and Figure 4.12. It is possible to compare the microstructure formation obtained with the SEM analysis with the literature, in Figure 2.21. The white matrix corresponds to the γ-matrix and the black spots to the γ'-phase. The faster growth of γ'-phase generates a more fragile region in which the crack starts. There are two possibilities for the formation of such regions: overheating and uneven heat flow. Both phenomena produce a region more suitable for the growth of γ'-phase. According to Göbenli [57], he γ'-phase is a fragile precipitate, which achieves a volume fraction up to 70 % in SX alloys. In Figure 4.11 is possible to observe the heterogeneous growth of this phase. The larger precipitates are fragile and more suitable to crack. Once the crack begins, the SX microstructure is convenient for the growth since there are no grain barriers to stop it. For this reason most of cracks cross the clad completely. The defects may be characterized as cold cracking according to the detailed view in Figure 4.12, where the break of γ-matrix is a signal of stresses by solidification.

Figure 4.10 – SEM analysis – I.

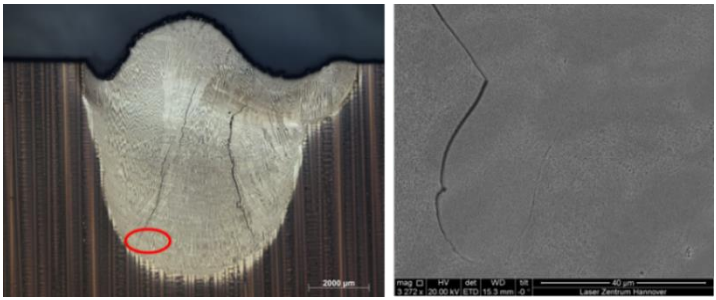

SOURCE: The author.

Figure 4.11 – SEM analysis – II.

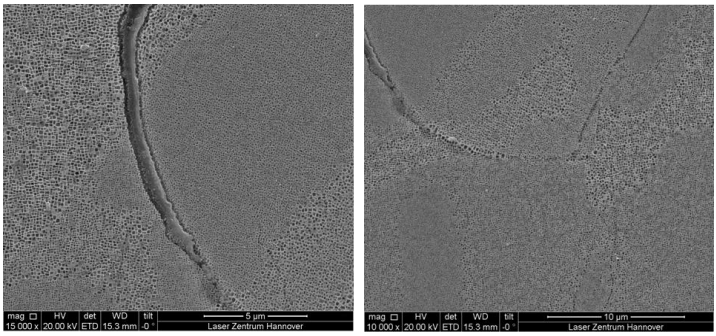

SOURCE: The author.

Figure 4.12 – SEM analysis – III.

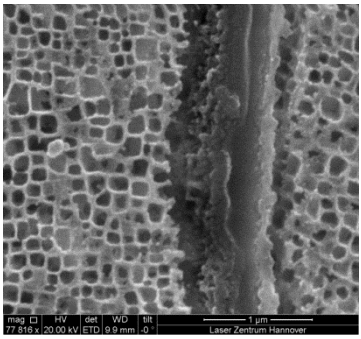

SOURCE: The author.

Another interesting point to approach is the region where the crack begins. Most of the samples have the larger cracks in the fusion line region. Since is used laser cutting to introduce the notch into the substrate, it is possible that the high process temperature introduces stresses in this region. However, a stronger hypothesis is that the uneven heat distribution (Figure 4.8) induces a temperature gradient to the lateral region from the notch. This changes the solidification from epitaxial to equiaxial, as presented in Figure 4.14. It is possible to identify the formation of new grains as the boundaries with different dendrite orientations.

Figure 4.13 – SEM analysis – IV.

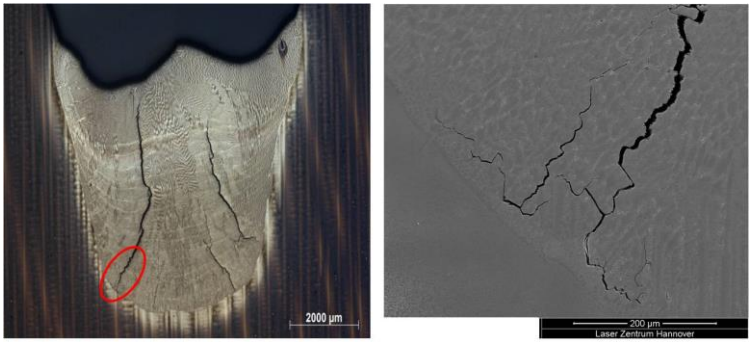

SOURCE: The author.

Figure 4.14 – SEM analysis – V.

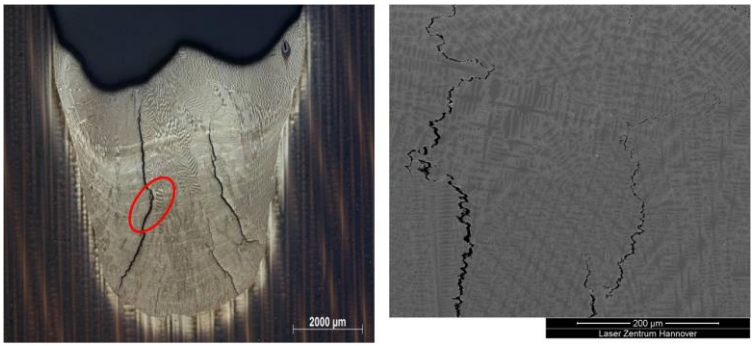

SOURCE: The author.

Preheating influence

The preheating was widely used into the clad on notch process with the objective to avoid the crack formation. The samples were preheated by means of a thermal induction coil positioned 1 mm away. The metallography results have shown a different microstructure, where the dendrite grows occurs no longer in the temperature gradient direction.

The thermal induction experiment evaluates the influence of the thermal induction on the process. The main idea is to submit the exactly same parameters of the best clad to the magnetic induction as preheating. For this, the parameter TE2 (chapter 4.2.2) is used as reference to comparison. The new samples are preheated with 1500 and 2500 W (PH1 and PH2, respectively), which corresponds to 650 and 820°C (Table 4.28).

Table 4.28 – Process parameters.

SA	BR [mm]	SS [mm/min]	CD [mm]	TE [°C]	PD [g/min]	PH [°C; W]
TE2	0,396	100	4	1400	3	-
PH1	0,396	100	4	1400	3	1500; 650
PH2	0,396	100	4	1400	3	2500; 820

SOURCE: The author.

In Table 4.29 are shown the metallography results. The use of thermal induction helps to avoid the asymmetric form, which is corrected due to more adhesion. It is more explicit in the sample PH2, where the clad width corresponds to the substrate lateral dimensions until the top. However, the magnetic induction clearly introduces an effect on the grain orientation. Exactly the same parameters that built a single-crystal clad without preheating, now present a disordered microstructure.

Table 4.29 – Metallography of samples with and without thermal induction.

	TE2	
	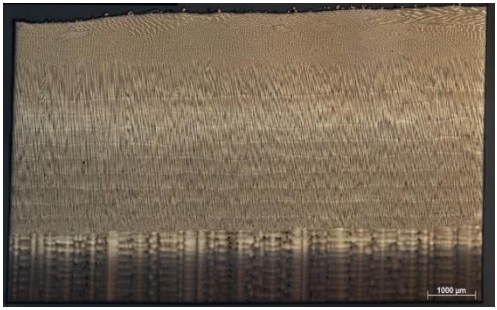	
	PH1	
	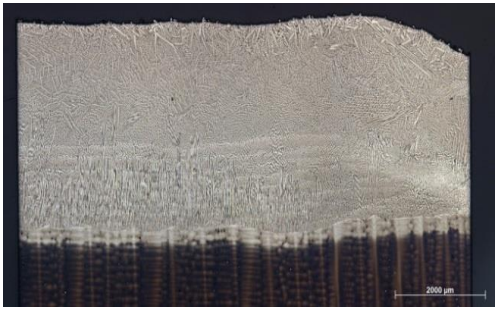	
	PH2	
	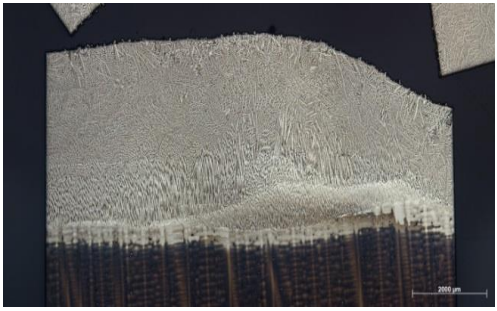	

SOURCE: The author.

An experimental assembly is build up to measure the intensity of the magnetic field, as presented in the Figure 4.15 scheme. The solenoid

measures the voltage and the frequency 2 mm away from the induction coil, as in the experiments. The magnetic field can be calculated according to Eq. (7), where B_s is the magnetic field intensity, U_{is} and f are the coil voltage and frequency, N_s the number of solenoids and r_s the distance from the solenoids to the induction coil.

Figure 4.15 – Magnetic field measurement.

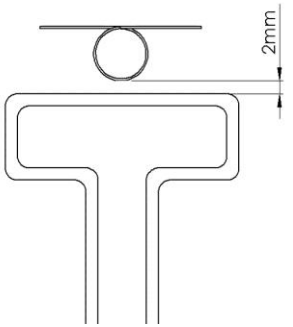

$$B_s = \frac{U_{is} \cdot 2 \cdot \frac{1}{f_s}}{N_s \cdot {r_s}^2} = \frac{3{,}8 \cdot 2 \cdot 5{,}4}{4 \cdot 6{,}55^2} = 0{,}24\ T \quad (7)$$

Where,

B_s - Magnetic field intensity
U_{is} - Coil voltage
f_s - Frequency
N_s - Number of solenoids
r_s - Dist. from solenoid to coil

SOURCE: Erbrecht [75].

The dendrite can be part of either a columnar or an equiaxed grain structure, depending of the working field. It is usual the appearance of an equiaxed zone at the end of columnar grain, which is known as the columnar-to-equiaxed transition (CET) [76]. According to *Li* [77], the application of a strong magnetic field causes a dendrite fragmentation and then the CET. A torque is created on the dendrites and equiaxed grains, which breaks it and drives the grain rotation. By a

critical level of magnetic field, the growth of columnar dendrites is blocked and the CET occurs. His experiment consists of nickel base alloys DZ417G samples with 3 mm of diameter and length of 200 mm manufactured with directionally solidified grains according to the Brigman method (Figure 2.26). A superconducting magnet can produce an axial static magnetic field with adjustable intensity up to 14 T. In Figure 4.16 is shown the results without (left) and with (right) application of a 10 T magnetic field [76].

Figure 4.16 – Nickel base alloy DZ417G directionally solidified without (left) and with (right) a magnetic field.

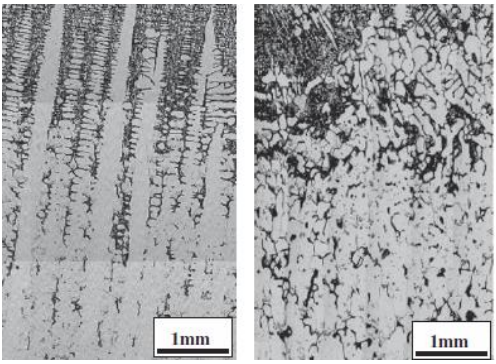

SOURCE: Ren *et al*. [76].

Ren *et al.* [77] has studied the effect of magnetic field on precipitation phases of single-crystal nickel-base superalloy during the directional solidification, which may be analyzed through the nucleation activation energy:

$$\Delta G = \frac{16\pi\sigma_{\gamma-\gamma'}^3}{3(\Delta G_V - \Delta G_\varepsilon)^2} \quad (8)$$

Where,

ΔG^* - Nucleation activation energy
$\sigma_{\gamma-\gamma'}$ - Interface energy between phases
ΔG_V - Volume free energy difference
ΔG_ε - Strain free energy difference

SOURCE: Li [77].

$$\Delta G = \frac{16\pi\sigma_{\gamma-\gamma'}^{3}}{3(\Delta G_V + \Delta G_M - \Delta G_\varepsilon)^2} \quad (9)$$

Where,

ΔG^* - Nucleation activation energy
$\sigma_{\gamma-\gamma'}$ - Interface energy between phases
ΔG_V - Volume free energy difference
ΔG_M - Magnetic free energy difference
ΔG_ε - Strain free energy difference

SOURCE: Li [77].

Where $\sigma_{\gamma-\gamma'}$ is the interface energy between γ' and γ phase, ΔG_V the volume free energy difference and $\Delta G\varepsilon$ the strain free energy difference (Eq.7). When the magnetic field is applied, the ΔG_M is added (Eq.8). It has been evidenced that the magnetic field application reduces the nucleation activation energy and thus causes the γ' phase refinement, which leads to the CET.

The thermal induction has a significant influence on the dendrite growth. This is observed by both nickel base alloys, CMSX-4 and DZ417G, with magnetic fields of 0,24 T and 10 T, respectively. The immense difference between both magnetic fields is compensated by the sample size. *Li* uses an ingot (3 mm of diameter and 200 mm length) and the CMSX-4 is introduced to the laser cladding process as powder with fine mesh (diameter between 45-100μm). Despite the differences between both processes, the results are similar and substantiates the reason why the induction preheating influences the process and disturb the dendrite growth.

5 CONCLUSIONS

The application of laser cladding as repair method for damaged turbine blades was performed according to different procedures. First was executed a study of the influence from base parameters. In the second stage the clad is enhanced to complete the surface of the sample. In the last experimental group corresponded to the cladding on a notch, which requires another approach due to different process characteristics.

Three methods were used to evaluate the microstructure obtained. The first method is the metallography, which permits to visualize the presence of cracks or grain disorientation. It proved to be very useful to identify the solidification path in the samples, as shows the comparison with the electron backscattered diffraction (EBSD). Some samples are also evaluated with the scanning electron microscopy (SEM) to verify problems concerning the clad formation.

The conclusions about each experimental group are exposed separately in order to evidence its results.

Preliminary tests

The preliminary tests corresponded to the evaluation of four parameters: beam radius (BR), scanning speed (SS), cooling distance (CD) and laser beam intensity (LI). It comprehends a study of base parameters in order to define the working range of the process.

The beam radius was modified in order to change the laser beam focus position relative to the nozzle powder convergence. There are three basic laser focus configurations: above, coincident, and after the powder convergence. It modifies the energy intensity, profile and diameter of the laser beam on the melt pool (Figures 3.9 until 3.13). The coincident point for the laser beam focus and the nozzle powder convergence results on the smaller diameter and higher energy concentration. According to Gedda [36], a signal of a good cladding is a small layer of remelted material in the substrate, which can be reported at BR3 configuration (Table 4.2). In addition to this, it presented a better result due to better PUR (Powder Usage Ratio) values and less substrate damage.

In laser cladding, the scanning speed is directly linked with the energy and quantity of powder delivered to the working area, according to Vilar *et al.* [35]. The higher the laser head speed on each track, the smaller is the amount of powder injected and energy per area, which results on the building of smaller clad walls. This assumption could be observed in the experiments from SS1 to SS4, where this characteristic

is noticed in the metallography samples from Table 4.5. The single-crystal microstructure could be better achieved using the scanning speed of 100 mm/min. Although the four parameter tested could be used to the process.

The variation of cooling distance is realized in order to simulate the manufacture of turbine blades as the standard process described by Steinhaus [59]. For that reason, this experiment is evaluated from 2 to 7 mm and by two different laser powers. The results have shown that from 2 to 5 mm is possible to achieve the single crystal structure. According to Turnbull [49], the energy barrier ΔG for the crystal to nucleate on the substrate will decrease with the increase of undercooling. For that reason, the smaller the distance between substrate surface and cooling plate, the higher the undercooling. This explains the better results observed for the smaller distances. Further experiments are performed with a distance of 4 mm, in order to improve the temperature gradient and permit an epitaxial solidification. On the other hand, the distance to the cooling plates barely influences the PUR results because the energy input is basically the same. This is reinforced by equation (4), from Kaiele *et al* [33], which set the scanning speed and laser power as parameters to define the energy input per unit length.

The last parameter experiments correspond to the laser beam intensity in the melt pool. The amount of energy applied on the process modifies completely the clad formation, which varies the clad form from concave to convex. It also influences the formation of the molten bath, which can be homogeneous and melt all the powder injected or, in extreme cases, melt the previous layers formed. This behavior was expected according to observations from Vilar *et al.* [35]. A consequence of such influence is the change of the PUR values, which normally increase together with the laser intensity.

With the results of the preliminary tests is possible to link the clad formation to the change of parameters for the laser cladding of CMSX-4. This information is used as background to the experiments involving the clad on top and on notch of samples.

Clad on top

The second phase of tests comprehends the application of the optimized parameters from the preliminary tests into the clad over the surface of the substrate, which corresponds to the repair of the abrasive damage on the top of the turbine blade. For that, the first tests concerned the investigation of the best strategy to the “clad on top” experiments. Due to the cost of each specimen, the first attempts were developed to

use just half of its length. However, the clad was not good enough to provide a homogeneous pattern. For that reason, it was chosen to perform the clad over the entire surface.

A significant modification in this battery of experiments is the use of a PID program to set the local temperature of the melt pool, which avoids the overheating and lack of energy in the process. Initially was evaluated the melt pool temperature with three different temperatures: 1350, 1400 and 1450°C. All of them could achieve the main objective of a single-crystal microstructure without pores or cracks. The implementation of a control system to adjust the laser beam intensity according to the temperature presented better results than with fixed laser beam intensity. The reduction of dilution levels minimize the effect in previous layers and enhance the microstructure, as supposed by Kou [41]. However, on the cross section is possible to observe an asymmetry due to material loss on one side. This defect can be resultant of a not optimized quantity of powder introduced into the melt pool. This assumption was made based on Lugscheider *et al.* [34], which states that the powder quantity influences the geometry of the clad layers. According to Kou [41], either there is not enough energy to melt all the powder or too much energy, which causes the dilution of previous layers and deforms the clad. To evaluate this mechanism, an experiment of powder quantity was performed with 2 and 4 g/min. The results showed that it affects directly the clad formation. The use of 2 g/min has shown a similar clad to the previous with 3 g/min, but without the lateral defect. The minimized quantity of powder delivered to the melt pool proportionate a uniform clad.

The clad is analyzed with the EBSD method, which confirms the mainly epitaxial solidification without cracks or pores. Some regions present grain misorientation, even with the presence of a temperature gradient during the experiments induces the epitaxial grain solidification. Steinhaus [59], states the importance of a well defined temperature gradient in order to manufacture the epitaxial turbine blade. An unexpected energy deviation in the melt pool may have weaken the main solidification direction and caused the misorientation observed. This assumption is reinforced by the unstable PID system responsible for the control of laser power. It was observed that the pyrometer readings eventually present problems referent to light reflections on the melt pool. These failures affect the PID actions, which eventually set the wrong power to the laser source.

Another possible reason for the appearance of misorientations is the nucleation of new grains in the fusion line during machining

operations to prepare the sample. According to Kou [52], for the nucleation to happen there is the need of exposal to high temperatures, which occurs during the laser cutting process for the preparation of samples. The grains nucleated during the preparation grow in another direction, resulting on misorientation in the new clad.

Clad on notch

The last experimental group refers to the clad on notch, which is a method developed to optimize the crack repair on the top of turbine blades. It consists of cutting the damaged region with a known geometry in order to remove the crack. The main idea is to reduce the material consumption and minimize the production time. On the other hand, the cladding complexity is increased due to the energy distribution inside the notch. It happens because the heat flow occurs no longer in one dimension, but in two, since the heat propagates to the lateral area as well. This phenomenon generates a region suitable for crack formation due to residual stress resultant from tensile and compressive strength. In order to improve it, there is used a thermal induction to preheat the substrate by means of an electromagnetic field. This decreases the temperature gradient on the sides and reduces the residual stress.

To clad the notch, it is used a different strategy then with the clad on top. Three tracks are used instead of one in order to overlap them and fulfill it completely. According to Lugscheider *et al.* [34], the cladding with overlap of single tracks next to each other is considered another process parameter. In addition to this, between two overlapping tracks is introduced a heat-affected zone (HAZ). However, one single track was not able to fulfill the sample thickness and a multi-track cladding is required.

The first experiments consisted of importing the parameters previously used to clad the substrate top. The same process was repeated with and without the substrate preheating. The results have shown that the use of thermal induction cooperates with the reduction of residual stress, since the clad presents no crack; on the other hand, the electromagnetic field generated by the induction coil affects the dendrite growth. According to *Li* [77], the application of a strong magnetic field causes a dendrite fragmentation and then the columnar-to-equiaxed transition (CET). In order to reinforce this assumption, an experiment from the “clad on top” trials is selected to be evaluated with and without the preheating. The results clearly shows that, even a considerably small magnetic field of 0,24 T, the SX solidification of CMSX-4 is disturbed.

Because of this unexpected magnetic field influence, the use of preheating has to be avoided. To overcome this situation, parameters change (laser beam intensity, scanning speed and laser beam radius) were tested in order to reduce the layer thickness and the interaction with the lateral area. This procedure is made to reduce the HAZ predicted by Lugscheider *et al.* [34] and Xiangling *et al.* [42]. However, the results have shown that such change is not enough to produce an epitaxial clad without cracks. The parameter change is not effective to produce a single-crystal clad. The results consist either of SX-microstructure with cracks (without preheating) or the polycrystalline crack free (with preheating). In order to find out a point between these two problems, several clad strategies were evaluated. They basically do not differ on process parameters, but how the preheating and cooling actuate in the system. Since the preheating is capable to eliminate the crack formation, the experiments concern to preheat the substrate with the thermal induction, but reduce the effects of the electromagnetic field during the cladding. The best result is using a support, which fix the sample, over the cooling plates. This strategy reduced the temperature gradient and permitted the substrate to maintain the preheating during the cladding. However, the crack formation could not be avoided.

In order to analyze the crack formation, Scanning Electron Microscopy (SEM) is used to evaluate the samples. It is possible to observe the crack origin in regions where the γ'-phase has achieved larger dimensions. According to Göbenli [57], it corresponds to the hard and brittle part of the microstructure, which is fragile and consequently suitable for the crack beginning. According to Xiangling *et al.* [42], the HAZ is under tensile stress, which results in premature failure. In this case, the failure occurs just after the clad due to the higher residual stresses achieved during the solidification, due to the heat exchange to the laterals of the notch.

The clad on notch could not be successfully performed with the methodology suggested in this work. The notch introduces a system suitable to the appearance of residual stress, which occurs basically because of the energy loss to the lateral region. The solution proposed to use a magnetic induction reduces the problems with residual stress, but causes the grain misorientation during the solidification, which is unacceptable for the epitaxial solidification.

Recommendations and Suggestions

From this work is possible to conclude that the use of laser cladding with powder delivery is suitable as a method to rebuilt parts of

CMSX-4 SX components. This can be proved by the results of the clad on the top of substrate, which are crack free and present epitaxial solidification required. However, the repair of cracks by the fulfillment of the notch could not be achieved. Some key point should be investigated in order to reach all the project objectives:

- Detailed study about the heat flow in the clad to have a homogenous energy dissipation and avoid regions with different precipitate (γ'-phase) concentration

- A preheating method that does not generates a magnetic field, for example ceramic plates or an hybrid process with laser preheating

- Work with larger laser beam diameters to reduce from multi- to single-track strategies and avoid the HAZ

- Preheated powder inside the nozzle

- Investigate the method to prepare the samples. Test the notch machining with a mechanical process (milling, for example) instead of laser cutting to avoid the nucleation of new grains

REFERENCES

[1] POLLOCK, T.; TIN, S. Nickel-based superalloys for advanced turbine engines: chemistry, microstructure and properties. **Journal of Propulsion and Power**, v. 22, n.2, March-April 2006.

[2] SIMS C.T.; STOLOFF N.S.; HAGEL W.C. **Superalloys II**. 2nd edition, Wiley, New York, 1987.

[3] BRÄUNLING, W. J. G. **Flugzeugtriebwerke**, Springer-Verlag, ISBN 978-3-540-76368-0, 2009.

[4] DURAND-CHARRE M. **The microstructure of superalloys**, Gordon and Breach, Amsterdam, 1997.

[5] GÄUMANN, M.; *et al*. Epitaxial laser metal forming: analysis of microstructure formation. **Materials Science and Engineering**, A271, p. 232-241, 1999.

[6] BÜRGEL, R. **Handbuch Hochtemperatur Werkstofftechnik: Grundlagen, Werkstoffbeanspruchungen, Hochtemperaturlegierungen und Beschichtungen**, Vieweg, ISBN 3–528–23107–6, 2006.

[7] TOYSERKANI, E.; KHAJEPOUR, A.; CORBIN, S. **Laser cladding**. CRC Press, 2005.

[8] HITZ, B; EWING, J. J.; HECHT J. **Introduction to laser technology**. Institute of Electrical and Electronics Engineers (IEEE), Inc. 2001.

[9] Avaiable at: <http://www.ophiropt.com/user_files/laser/beam_profilers/What-is-m2.pdf>
Date acessed: 01.05.2014.

[10] Avaiable at: <http://www.rp-photonics.com/m2_factor.html>
Date acessed: 01.05.2014.

[11] KAIERLE, S. Laser in der Biomedizintechnik. **Lecture: Leibniz Universität Hannover**, 2013.

[12] PATEL, C. K. N. **Continuous-wave laser action on vibrational-rotational transitions of CO_2.** Phys. Rev. 136 (5A), A1187, 1964.

[13] TÜNNERMANN, A. *et al*. **Fiber lasers and amplifiers:** an ultrafast performance evolution. 2010.

[14] CHAOYANG, L. *et al*. H**igh beam quality diode-side-pumped Nd:YAG**. Opt. Express 18 (8-7923), 2010.

[15] ENDRIZ J. G. *et al.* **High power diode laser arrays.** IEEE Quantum Electron, 28 (4-952), 1992.

[16] DIEHL R. **High-power diode lasers:** fundamentals, technology, applications. Springer, Berlin, 2000.

[17] BOTEZ D.; SCIFRES D. R. **Diode Laser Arrays.** Cambridge University Press, Cambridge, 1994.

[18] POWELL J.; HENRY P.S.; STEEN W.M. Laser cladding with preplaced powder: Analysis of thermal cycling and dilution. **Surface Engineering**, v. 4, n^{o}. 2, p. 141-149, 1988.

[19] MEINERS, W. **Direktes Selektives Laser Sintern einkomponentiger metallischer Werkstoffe.** Shaker Verlag, Aachen, 1999.

[20] DRAUGELATES, U. *et al*. **Corrosion and wear protection by CO_2 laser beam cladding combined with the hot wire technology.** ECLAT , p. 344-354, 1994.

[21] STEENBERGEN, M. **Ontwerp en Realisatie van een Draadtoevoersysteem voor Lasercladden.** University of Twente, Dept. of Mechanical Engineering, 1993.

[22] WOLF, S. *et al*. Laserstrahlbeschichten nach der Einstufigen Prozeßführung am Beispiel "Beschichten von Gußeisen".**Laser und Optoelektronik**, v. 26, n^{o}. 4, p. 63-67, 1994.

[23] VOLZ, R.; MAISENHÄLDER, F. Beschichten von Stahl- und Kupfersubstraten mit CO_2-Hochleistungslasern nach der Einstufigen Prozeßführung. **Materialbearbeitung mit CO2-Laserstrahlen höchster Leistung**, VDI, Düsseldorf, p. 73-79, 1994.

[24] CARVALHO, P. A. *et al*. Automated workstation for variable composition laser claddin: use for rapid alloy scanning. **Surface and Coatings Technology**, v. 72, p. 62-70, 1995.

[25] WECK, M.; SCHÖN, J. Integration prozeßspecifischer Sensoren und Aktoren in das Strahlführungssystem – Arbeitskopf mit Wechselobjektiv für das Oberflächenveredeln. **Materialbearbeitung mit CO_2-Laserstrahlen höchster Leistung**, p. 105-110, 1994.

[26] HURON, E.S. Serrated Yielding in a Nickel-Base Superalloy. **Superalloys** 1992, TMS, Warrendale, PA, p. 675–684, 1992.

[27] ISLAM, M.U.; XUE L.; MCGREGOR G. **Process for manufacturing or repairing turbine engine or compressor components.** U.S. Patent Number 6269540, 2001.

[28] JEANETTE P.F. *et al*. **Multiple and system for producing complex-shape objects.** U.S. Patent Number 6046426, 2000.

[29] NOWOTNY, St. . COAXn: Modular system of powder nozzles for laser beam build-up welding. **Proceeding of ICALEO**, LMP Section pp. 190-193. LIA, 2003.

[30] LIN, J. A simple model of powder catchment in coaxial laser cladding. **Optics and Laser Technology,** v. 31, n. 1, p. 233-238, 1999.

[31] KOMVOPOULOS, K.; NAGARATHNAM, K. Processing and characterization of laser-cladded coating materials. **Journal of Engineering Materials and Technology**, v. 112, p. 131-143, 1994.

[32] KREUTZ, E. W. *et al*., Rapid prototyping with CO2 laser radiation. **Applied Surface Science 86**, p. 310-316, 1995.

[33] KAIERLE, S. *et al*. Review on laser deposition welding: from micro to macro. **Physics Procedia**, n. 39, p. 336-345, 2012.

[34] LUGSCHEIDER, E.; OBERLÄNDER, B. C.: LEISING, S. E. Influence of laser cladding parameters on the microstructure and properties of claddings. **Surface Modification Technologies V**, Aachen University of Technology, p. 880-888, 1992.

[35] VILAR, S.; NETO, D.; Interaction between the laser beam and the powder laser alloying and cladding. **Conference proceedings ICALEO 98,** Orlando, USA.

[36] GEDDA, H. **Laser surface cladding**: a literature survey. Luleå University of Technology, ISSN: 1402-1536, ISRN: LTU-TR—00/07-SE, 2007.

[37] FRENK, A. *et al.* Analysis of the laser cladding process for satellite on steel. **Metallurgical and Material Transactions B**, vol. 28B, p. 501-508, 1997.

[38] SCHNEIDER, M. **Laser cladding with powder**, Universiteit Twente, Ph. D. Thesis, 1998.

[39] BRENNER, B.; REITZENSTEIN, W. Laser hardening of turbine blades. **Industrial Laser Review**, p. 17-20, 1996.

[40] EIGENMANN, B. Residual stresses due to thermal, thermo-chemical and mechanical surface treatments: generation, determination, evaluation. **Proc. Surface Treatment 95**, p. 17-25, 1995.

[41] KOU, S. **Welding metallurgy:** Residual stress in weldments. ISBN 0-471-84090-4, p. 100-113, 1987.

[42] XIANGLIN, Z.; HANQI, H.; JIAHONG, Y. Residual thermal stresses of laser cladding of intermetallic ceramic composite

coatings. **Journal of University of Science and Technology**, v. 4, n 2:31, p. 31-33, Beijing.

[43] BRUCK, G. J. High power laser beam cladding. **Journal of Metals**, v. 39, n. 2, p. 10-13, 1987.

[44] STEEN, W. M. Laser surface cladding, **Proc. Surtek-4**, p. 159-166, 1987.

[45] POLLOCK, T. M.; FIELD, R. D. Dislocations and high temperature plastic deformation of superalloy single crystals, **Dislocations in Solids.** v. 11, p. 549–618, Amsterdam, 2002.

[46] GÄUMANN, M. *et al*, Single crystal turbine components repaired by epitaxial laser metal forming. **Materials for Advanced Powder Engineering**, v. 1479, p. 1-6, 1998.

[47] SHEPELEVA, L. *et al*, Laser cladding of turbine blades. **Surface and Coatings Technology**, v. 125, n. 1, p. 45-48, 2000.

[48] TANAKA, Y. *et al*, Large engine maintenance technique to support flight operation for commercial airlines, **Technical Review**, Mitsubishi Heavy Industries Ltd., v. 40, n. 2, 2003.

[49] TURNBULL, T. J. **Chem. Physiol**, 18:198, 1950.

[50] SAVAGE, W. F. *et al*. **Weld Journal**, 51:260s, 1972.

[51] ELMER, J. W.; ALLEN, S. M.; EAGAR, T. W. **Metall. Trans. A**, 20A:2117, 1989.

[52] KOU, S. **Welding metallurgy**. ISBN 0-471-43491-4, ed. 2, 2002.

[53] ILSCHNER, B.; SINGER, R. **Werkstoffwissenschaften und Fertigungstechnik: Eigenschaften, Vorgänge, Technologien**. Springer, ISBN 978–3–642–01733–9, 2010.

[54] WEISSBACH, W. **Werkstoffkunde: Strukturen, Eigenschaften, Prüfung**. Vieweg, Teubner Verlag, ISBN 978-3-8348-1587-3, 2012.

[55] ESSER, Dr. W. **Einkristallschaufeln für stationäre Gasturbinen.** Turbinenschaufeln aus Einkristallwerkstoffen, Abschlussbericht 03 M 3038 C, Siemens AG, Energieerzeugung KWU, Mühlheim an der Ruhr, 1997.

[56] RITZENHOFF, R. **Beeinflussung der Erstarrungsbedingungen von Nickelbasis Superlegierungen und Auswirkung auf die mechanisch-technologischen Eigenschaften**. Thesis – Faculty of Materials Science, Technischen Universität Bergakademie Freiberg, 2007.

[57] GÖBENLI, G. **Werkstoffwissenschaftliche Untersuchungen zum ein- und mehrachsigen Kriechverhalten der Nickelbasis-Superlegierungen CMSX-4 und LEK 94 oberhalb 1000 °C.** Thesis – Department of Mechanical Engineering, Ruhr-Universität Bochum, 2005.

[58] VEHN, M. **Unterkühlungsbedingte Gefügeinhomogenitäten einkristallin erstarrter Turbinenschaufeln.** Thesis – Faculty of Mining, Metallurgy and Science, Rheinisch-Westfälischen Technischen Hochschule Aachen, 1997.

[59] STEINHAUS, T. **Validierung des nichtlinearen Verformungsverhaltens von großen Einkristall-Gasturbinenschaufeln aus CMSX-4**. Thesis – Department of Mechanical Engineering, Rheinisch-Westfälischen Technischen Hochschule Aachen, 2001.

[60] BROCKHAUS, R.; ALLES, W.; LUCKNER, R. **Flugregelung.** Springer-Verlag, ISBN 978-3-642-01442-0, 2011.

[61] WAGNER, I. A. **Einkristallerstarrung stark lokal unterkühlter Superlegierungsschmelzen (Autonome Gerichtete Erstarrung)**. Shaker Verlag, ISBN 3-8265-8560-7, 2001.

[62] WEIDLICH, N. **Individual laser cladding for high pressure turbine blades**. VDI-Berichte, n. 2028, 2008.

[63] KATHURIA, Y.P. Some aspects of laser surface cladding in the turbine industry. **Surface and coatings technology**, v. 132, n. 2-3, p. 262-269, 2000.

[64] LORIA, E. A. **Superalloy 718:** metallurgy and applications. TMS, Warrendale, PA, 1989.

[65] GASSER, A.; *et al*. Laser metal deposition (LMD) and selective laser melting (SLM) in turbo-engine applications. **Laser material processing**, Laser-Journal, 2010.

[66] MURAKUMO, T. *et al*. Creep behavior of Ni-base single-crystal superalloys with various gamma' volume fraction. **Acta Materialia**, v. 52, n. 12, p. 3737–3744, 2004.

[67] RAE, C. *et al*. On the primary creep of cmsx-4 superalloy single crystals. **Metallurgical and materials transactions A**, v. 31A, n. 9, p. 2219-2228, 2000.

[68] SHYAM, A. *et al*. Development of ultrasonic fatigue for rapid, high temperature fatigue studies in turbine engine materials. **Superalloys**, TMS, p. 259–267, Warrendale, PA, 2004.

[69] WRIGHT, P. ; JAIN, M.; CAMERON, D. High cycle fatigue in a single crystal superalloy: time dependence at elevated temperature. **Superalloys** , TMS, p. 657–666, , Warrendale, PA, 2004.

[70] WERNER, A. **Verschleißphänomene im Flugzeugbau**, MTU Aero Engines. Avaiable at: <http://www.mtu.de/de/technologies/engineering_news/Werner_Verschleissphaenomene_im_Flugtriebwerksbau_de.pdf> Date acessed: 17.08.2013.

[71] **Laser safety manual**. Seattle: University of Washington, 2007.

[72] IEC 60825-1: **Safety of laser products.**: International Electrotechnical Comission, Geneva, 2001.

[73] DEACON, R. M. Metallography, microstructure and analysis. **Application and Innovation for Metals, Alloys and Engineered materials journal**, n 13632, ISSN: 2192-9270, 2014.

[74] Available at: <http://serc.carleton.edu/research_education/geochemsheets/ebsd.html>
Date acessed: 05.05.2014.

[75] ERBRECHT, R. *et al*. **Das große tafelwerk.** ISBN 3-06-020760-7, Berlin, 1999.

[76] REN, W. *et al*. The effect of magnetic field on precipitation phases of single-crystal nickel-base superalloy during directional solidification. **Material letters**, n°. 100, pp. 223-226, 2013.

[77] LI, X. *et al*. Dendrite fragmentation and columnar-to-equiaxed transition during directional solidification at lower growth speed under a strong magnetic field. **Acta materialia**, n. 60, p. 312-3332, 2012.